

Obstruction to ergodicity in nonlinear Schrödinger equations with resonant potentials

Anxo Biasi¹, Oleg Evnin^{2,3}, Boris A. Malomed^{4,5}

¹*Laboratoire de Physique de l'École Normale Supérieure ENS Université PSL, CNRS, Sorbonne Université, Université de Paris, F-75005 Paris, France*

²*Department of Physics, Faculty of Science, Chulalongkorn University, Bangkok 10330, Thailand*

³*Theoretische Natuurkunde, Vrije Universiteit Brussel and International Solway Institutes, Brussels 1050, Belgium*

⁴*Department of Physical Electronics, School of Electrical Engineering, Tel Aviv University, Tel Aviv 69978, Israel*

⁵*Instituto de Alta Investigación, Universidad de Tarapacá, Casilla 7D, Arica, Chile*

We point out a class of trapping potentials in nonlinear Schrödinger equations that make them non-integrable, but prevent the emergence of power spectra associated with ergodicity. The potentials are characterized by equidistant energy spectra (e.g., the harmonic-oscillator trap), and therefore by a large number of resonances enhancing the nonlinearity. In a broad range of dynamical solutions, spanning the regimes of both weak and strong nonlinearity, the power spectra are shaped as narrow (quasi-discrete) evenly spaced spikes, unlike generic truly continuous (ergodic) spectra. We develop an analytical explanation for the emergence of these spectral features in the case of weak nonlinearity. In the strongly nonlinear regime, the presence of such structures is tracked numerically by performing simulations with random initial conditions. Some potentials that prevent ergodicity in this manner are of direct relevance to Bose-Einstein condensates: they naturally enter 1D, 2D and 3D Gross-Pitaevskii equations (GPEs), the quintic version of these equations, and a two-component GPE system.

I. INTRODUCTION

The clash between integrability and ergodic behavior is a well-known phenomenon [1, 2]. While dynamics of generic systems with many degrees of freedom typically exhibit thermalization, chaotization and stochasticity, dynamics of integrable systems are tightly constrained by a large (or infinite) number of conservation laws. A conflict between these two distinct pictures arises when the system is “close” to integrability [1]. In that case, a natural question is to what extent the dynamics will display ergodic features. Such questions were raised, in particular, two decades ago by experiments with nearly-1D cold atomic gases [3, 4] because the underlying basic model may be the integrable Lieb-Liniger one [5], but integrability-breaking effects cannot be completely eliminated from the real-world setup. This problem motivated the study of deviations from the standard framework of non-equilibrium dynamics [6], bringing along intriguing ideas such as generalized hydrodynamics [7–13], prethermalization [14–17], generalized Gibbs ensembles [18–20], etc.

A common approach to analytical and numerical studies of the above questions relies on perturbing an integrable equation by extra terms – typically, this is an external trap added to the nonlinear Schrödinger equation (NLSE) [10, 21]. Then, one explores the consequences of integrability breaking in the perturbed model [10, 11, 17, 21–23]. One may, however, wonder whether *a mechanism other than integrability* exists to produce essential deviations from ergodic signatures of non-integrable dynamics. This question underlies the present paper, leading to a class of NLSEs including *highly resonant potentials* (HRP), namely, ones that, for the linear Schrödinger equation, yield equidistant spectra

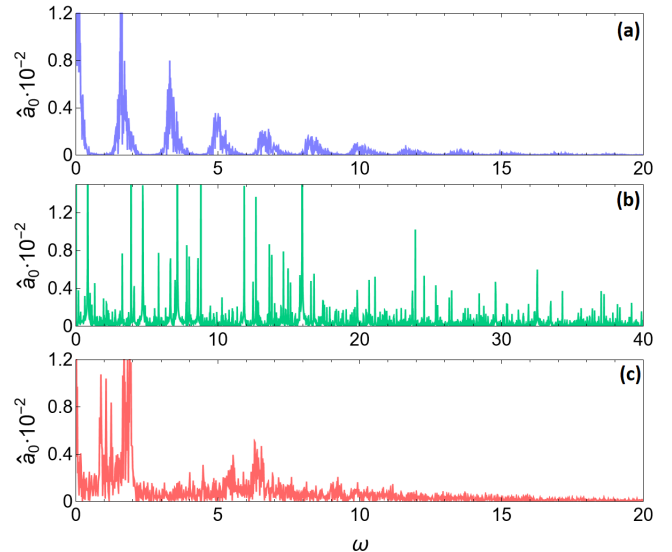


FIG. 1. The contrast between power spectra of the first-mode amplitude \hat{a}_0 , defined as per Eq. (11), as produced by the numerical solution of the one-dimensional NLSE in the HO potential (a), infinitely deep square potential well (b), and quartic potential (c), initialized by the input with a random phase and amplitude. Amplitudes of higher modes display similar plots.

of energy eigenvalues E_n :

$$E_n = an + b, \quad (1)$$

with integer n and real constants a and b . The most commonly known example is the harmonic-oscillator (HO) potential, whose equidistant spectrum is a consequence of the hidden symmetry of the respective quantum Hamiltonian. Similarly, the equidistant structure of spectra of other potentials is related to their symmetries [24].

The term *highly resonant* reflects extreme abundance of resonances in these systems. Indeed, the equidistant positioning of the eigenvalues in Eq. (1) ensures that the four-wave resonance condition, $E_n + E_m - E_l - E_j = 0$ with integers n, m, l, j , reduces to a simple relation between the integer numbers, $n + m - l - j = 0$, which implies an infinite number of resonances for any mode ($n = l + j - m$). It is shown below that the special structure of energy eigenvalues (1) has a strong impact on the dynamics, producing a regime of non-ergodic evolution, in contrast with the case of generic (non-equidistant) energy spectra. This phenomenon is demonstrated, in particular, by the power spectra presented in Fig. 1. In the case of generic trapping potentials, the system indiscriminately excites a large range of frequencies, which leads to ergodic (continuous and unstructured) power spectra [25], as shown in Figs. 1(b) and (c), which correspond, respectively, to the infinitely deep square well and anharmonic potential. By contrast, HRPs, in a parameter range spanning weakly and strongly nonlinear regimes, give rise to unusually depopulated power spectra, in which the excited frequencies reside in a “comb-like” arrangement of spikes, as shown in Fig. 1(a). The comb-like spectra induced by HRPs reveal an obstruction to ergodicity, being drastically different from the continuously distributed spectra created by generic traps. This conclusion is upheld by the similarity of the comb-like power spectra in HRPs to the discrete power spectra which are a characteristic feature of the integrable dynamics. They are associated with periodic and quasi-periodic trajectories that the integrable dynamics track on the surface of invariant tori in the phase space.

Our motivation to search for alternatives to exact integrability in explaining non-ergodic behavior came from specific results for the 1D Gross-Pitaevskii equation (GPE), which is a well-established model for the dynamics of atomic Bose-Einstein condensates, based on the NLSE for the mean-field wave function of the condensate [28–30]. It is commonly known that the NLSE is integrable in the free 1D space [31, 32], thus providing a good starting point for the study of the clash between integrability and ergodicity. The dynamical behavior in the presence of an external trap, which breaks integrability [33], has been addressed for non-equilibrium configurations [25, 34–40], coherent states in time-dependent traps [41, 42], and the propagation of a small number of solitons [43–52] (see also Refs. [53–61] for related models). Numerical works [43–46] suggested remarkable contrast between the GPE with the HO potential, and the equation including either anharmonic potentials or the infinitely deep potential box, which is represented by zero boundary conditions at the box edges. In particular, a single dark soliton trapped in the box potential displays a continuous power spectrum, in consonance with ergodicity and indicating the emission of radiation [46]. On the other hand, the evolution of the dark soliton governed by the GPE with the HO potential gives rise to a quasi-discrete power spectrum, reminiscent of discrete spectra

associated with the quasiperiodic dynamics of integrable systems [46]. The non-ergodic behavior of the 1D GPE with the HO potential, as opposed to the apparent ergodicity maintained by other potentials, is not restricted to the soliton motion, but also happens for more generic initial conditions, such as random waves. As shown in Fig. 1, the evolution initialized by these configurations in the case of the HO potential displays comb-like power spectra, while ergodic ones (truly continuous and unstructured) are seen in case of the box and quartic potentials. The specific shape of the power spectra supported by the HO potential suggests the presence of an underlying mechanism constraining the dynamics to a non-ergodic form. It was referred to as “quasi-integrability” in Ref. [46], because, as said above, discrete spectra are characteristic of integrable systems.

NLSEs with the HO potential display peculiar behavior which is not restricted to 1D. In particular, in 2D there are analytical solutions describing periodically modulated motion of a single-vortex [62] and multi-vortex configurations [63–65], as well as dark rings [64], or analytical and numerical manifestations of Fermi-Pasta-Ulam recurrences [65]. In Ref. [66], the rich structure exhibited by weakly nonlinear dynamics of the 2D GPE with the HO potential was extended to a large family of related systems with similar behaviors, and in Ref. [67], it was connected to the presence of breathing modes [68, 69]. Another setup where the HO potential has shown quasi-periodic motions is the 1D quintic NLSE [70].

The connection between the 2D GPE with the HO potential and other systems with equidistant linear spectra subject to condition (1), which were considered in Refs. [66, 67, 70] is an incentive to find out whether the quasi-integrability of the 1D GPE with the HO potential, established in Ref. [46], is an exceptional feature, or, on the contrary, it is shared by a large class of NLSEs. To this end, we examine the role played by the potential and conclude that comb-like power spectra similar to the one plotted in Fig. 1(a) are displayed by NLSEs with HRPs, whose linear spectra of energy eigenvalues take the form of Eq. (1). On the other hand, NLSEs with potentials that do not obey definition (1) do not display comb-like spectra, even if their spectra admit resonances between some modes.

Our results suggest three essential implications. First, NLSEs including HRPs constitute a broad class of models ranging from some of the most common and physically relevant ones, such as the GPE with the HO potential in any number of spatial dimensions, to more sophisticated potentials and nonlinear terms. The availability of 2D and 3D models of this type is particularly interesting for experiments because they overcome fundamental limitations inherent to studies of weakly broken integrable dynamics. First, the perturbation theory applies, in the traditional form, solely to 1D models [33]. The second lifted limitation, which is related to the first one, is that our models are not necessarily produced by deformations of integrable equations. An example is the 1D quintic

NLSE with the HO potential, which features non-ergodic power spectra without proximity to an exactly integrable equation (see details below). Finally, it is relevant to stress that our results offer an example of how a linear property, *viz.*, the equidistant linear energy spectrum (1), may impose a fundamental constraint on the full nonlinear dynamics, preventing the onset of ergodicity. For our exposition of the results we will mostly refer to two models, the 1D GPEs with the HO and box potentials, which represent the HRP and non-HRP, respectively. Then, we will explain how similar results are produced by other potentials of the same type.

The rest of the paper is organized as follows: First, we introduce the setup and make a direct comparison between the dynamics under the action of the HO and box potential. Then, we develop an analytical approximation for the power spectrum in the case of weak non-linearity, which makes it possible to explain differences between the respective power spectra. Afterwards, we show numerically how the comb-like power spectrum depends on the magnitude and sign (defocusing/focusing) of the nonlinear terms. This is followed by the presentation of comb-like power spectra produced by *eleven* other HRP models, which provide a robust confirmation of the genericity of our results. The paper is concluded by a discussion of the prospects and implications of our findings.

II. 1D GPES WITH THE HO AND BOX POTENTIALS

Throughout this paper, we use the 1D GPE as the main setup to illustrate the methods and results. In section V, we describe several other models, related to the ones addressed here. The scaled form of the NLSE is

$$i\partial_t\psi = -\frac{1}{2}\partial_x^2\psi + V(x)\psi + g|\psi|^2\psi \quad (2)$$

where $V(x)$ is the potential, and g the nonlinearity coefficient with $g > 0$ and $g < 0$ for the defocusing and focusing self-interactions, respectively. This equation conserves the norm

$$M = \int_{-\infty}^{+\infty} |\psi|^2 dx, \quad (3)$$

and energy (Hamiltonian)

$$H = \int_{-\infty}^{+\infty} \left(\frac{1}{2} |\nabla\psi|^2 + V(x)|\psi|^2 + \frac{g}{2} |\psi|^4 \right) dx, \quad (4)$$

which includes the quadratic and quartic parts, associated with the linear and nonlinear terms in Eq. (2), respectively:

$$H_2 = \int_{-\infty}^{+\infty} \left(\frac{1}{2} |\nabla\psi|^2 + V(x)|\psi|^2 \right) dx, \quad (5)$$

$$H_4 = \frac{g}{2} \int_{-\infty}^{+\infty} |\psi|^4 dx. \quad (6)$$

We fix the normalization by setting $M = 1$ in Eq. (3).

The HO and box potentials are our representative examples, chosen to illustrate the differences between HRP and non-HRP cases, respectively:

$$\text{HO} : V(x) = \frac{1}{2}x^2, \quad \text{box} : \begin{cases} 0, & \text{for } x \in (0, L), \\ \infty, & \text{elsewhere,} \end{cases} \quad (7)$$

where the coefficient of the HO potential is fixed by scaling to be 1, and L is the size of the box, and the Dirichlet boundary conditions $\psi(t, 0) = \psi(t, L) = 0$ are implied in this case. The linearized equations ($g = 0$) give rise to the commonly known eigenvalues E_n and eigenfunctions $f_n(x)$:

$$\text{HO} : E_n = n + \frac{1}{2}, \quad f_n(x) = \frac{H_n(x)}{\pi^{1/4}\sqrt{2^n n!}} e^{-x^2/2}, \quad (8)$$

$$\text{box} : E_n = \frac{\pi^2(n+1)^2}{2L^2}, \quad f_n(x) = \sqrt{\frac{2}{L}} \sin \frac{\pi(n+1)x}{L}, \quad (9)$$

where $n \geq 0$ is the number of the bound states, and $H_n(x)$ are Hermite polynomials. We fix $L = \pi/\sqrt{2}$ in order to make meaningful comparisons possible between power spectra in the HO and the box without an ambiguity in the frequency scale. The fact that the HO potential belongs to the class of HRPs is determined by its equidistant energy spectrum (8), while the quadratic spectrum (9) indicate that the box potential belongs to the non-HRP class, although it admits some resonances among its modes, much fewer than in the equidistant spectrum.

In both cases, the sets of eigenstates $f_n(x)$ are used to rewrite the solution to Eq. (2) in terms of complex mode amplitudes $\alpha_n(t)$, defined so that

$$\psi(t, x) = \sum_{n=0}^{\infty} \alpha_n(t) f_n(x) e^{-iE_n t}. \quad (10)$$

The most important quantity in this work is the power spectrum of the amplitudes,

$$\hat{a}_n(\omega) \equiv \mathcal{F} [|\alpha_n(t)|^2] \quad (11)$$

where \mathcal{F} stands for the Fourier transform. To produce $\hat{a}_n(\omega)$, we solve numerically Eq. (2) using the schemes outlined in Appendix A, and then identify amplitudes $\alpha_n(t)$ as per Eq. (10).

As initial conditions we use waves prepared with random phases and amplitudes, in the form of

$$\alpha_n(0) = \begin{cases} \mathcal{A}_n e^{i\mathcal{P}_n} & \text{for } n \leq \mathcal{N} \\ \mathcal{A}_n e^{i\mathcal{P}_n} e^{-\beta(n-\mathcal{N})} & \text{for } n > \mathcal{N} \end{cases} \quad (12)$$

where \mathcal{A}_n and \mathcal{P}_n are random numbers uniformly distributed in $[0, 1]$ and $[0, 2\pi)$, respectively, \mathcal{N} is the number of significantly excited modes, and $\beta > 0$ determines the suppression of higher modes. The set of initial amplitudes $\alpha_n(0)$ is scaled so as to satisfy the normalization, $M = 1$. We use the input (12) because the exponential suppression of the higher modes typically occurs

in configurations arising in the course of dynamical evolution. Each realization of input (12) features a different content of modes and phases, yielding an adequate form of generic (“natural”) initial states. Therefore, they provide an appropriate arena for formulating generic results. This approach brings in a broader perspective in comparison with focusing on special solutions, such as single solitons. In this regard, our simulations may actually be understood as the evolution of configurations given by superpositions of a large number of dark solitons, corresponding to notches in the pattern (the superposition also including other ingredients), as Fig. 2 suggests. Note also that random initial conditions similar to those given by Eq. (12) are used in studies of the wave turbulence [71], with the aim to produce a generic dynamical picture, rather than focusing on specific solutions. In particular, the 1D NLSE in a very broad box with periodic boundary conditions was used to study the dynamics of random waves in integrable equations [72–74] (the “integrable turbulence” introduced by Zakharov [75]), the formation of rogue waves [76–78], etc. In this context, our use of random initial configurations in the presence of trapping potentials follows the general framework adopted for the studies of spatially confined random waves.

A detailed visualization of the evolution of random waves in the HO and box potentials is produced, respectively, in the left and right columns of Fig. 2. In both cases, the evolution is affected by the strong nonlinearity and a broad wavelength spectrum of the initial excitation ($g = 250$, $\mathcal{N} = 20$, $\beta = 1$).

First, we dwell on the case of the HO potential. In this case, the condensate is initially localized at the center of the domain, marked with many notches. At the initial stage of the evolution, the condensate performs a sequence of alternating expansion-compression cycles associated with the action of the HO potential (Fig. 2I.a), and then relaxes to a spread state (Fig. 2I.b) that keeps a nearly constant envelope in time, together with a large number of notches shuttling from side to side, resembling a gas of solitons [79]. The relaxation process may be observed in the evolution of energy terms H_2 (5) and H_4 (6) in Fig. 2I.c. Their ratio, starting from a value $H_4/H_2 \approx 2.2$, initially oscillates with large amplitudes corresponding to expansion and compression of the condensate. After $t \approx 80$ the energy exchanges significantly subside, with the energies oscillating around nearly constant values in the course of the subsequent evolution, with the ratio $H_4/H_2 \simeq 0.42$, which is much larger than in the case of the weakly nonlinear regime ($H_4/H_2 \ll 1$). The power spectrum associated with this evolution scenario features the same peculiar comb-like shape presented in Fig. 1(a), as seen in Fig. 2I.e. While one might assume that this shape originates from the initial expansion-compression stage, the simulations are long enough to guarantee the completion of the system’s relaxation in the course of 20% of the total simulation time, while the stabilized stage of the evolution covers the

remaining 80% of the time. Moreover, omitting the relaxation stage in the computation of the power spectrum, its shape practically does not change. As concerns the propagation of dark solitons in the condensate, Figs. 2I.a-I.b exhibit their relatively smooth trajectories at both stages of the evolution, the expansion-compression and stabilized ones.

In the case of the box potential, Fig. 2II shows that the random-phase-and-amplitude input (12) fills the box from the beginning, remaining in this state at all times. We have also explored the case where the random-phase-and-amplitude input is localized at the center of the box. In that case, following the initial expansion, the condensate remains in the spread state, without featuring expansion-compression cycles. In the course of the evolution, the energies again oscillate around values with ratio $H_4/H_2 \simeq 0.42$. Taking close-by values of this ratio in the cases of the HO and box potentials is necessary, once the objective is to compare similar nonlinear regimes. In spite of the proximity of the ratio $H_4/H_2 \simeq 0.42$ in both cases, the action of the box potential leads to the emergence of a continuous (ergodic) power spectrum in Fig. 2, in contrast with its comb-shaped counterpart for the HO potential. It is also worthwhile to note a significant difference in the range of excited frequencies in the respective power spectra. We stress that the difference from the case of the HO potential is not a banal consequence of the mismatch in the box size because we have set $L = \pi/\sqrt{2}$ above precisely with the purpose to match linear energy spectra of both systems [$(E_n)_{\text{HO}} = n + 1/2$ and $(E_n)_{\text{box}} = (n + 1)^2$], and, as we show in the next section, this value of L is the only one that provides matching of positions of the excited frequencies in the power spectra of both systems. The ergodicity in the box potential has been previously observed in Ref. [25] for initial conditions that expand from the center, in agreement with our remark that there is no essential difference with the long-time evolution initialized by the input filling the entire domain. Analogously to the HO potential, dark solitons propagate throughout the box, but they do not follow smooth trajectories even in the interior of the box because of the multiple collisions between them, and shapes of individual solitons are identified less clearly.

We have also tested the presence of ergodicity in the case of non-HRPs whose generically shaped spectra of energy eigenvalues do not admit resonances. For instance, the 1D quartic potential, $V(x) = x^4/2$, is a non-HRP one, as shown by lowest eigenvalues numerically computed with accuracy $\Delta E_n \sim 10^{-4}$:

$$\begin{aligned} E_0 &= 0.5302, & E_1 &= 1.8998, & E_2 &= 3.7278, \\ E_3 &= 5.8224, & E_4 &= 8.1309, & E_5 &= 10.6192, \\ E_6 &= 13.2642, & E_7 &= 16.0493, & E_8 &= 18.9615. \end{aligned} \quad (13)$$

In this case, the input provided by random waves gives rise to an initial expansion-compression stage before relaxing to a spread state, similar to the dynamical scenario observed above under the action of the HO potential, but the power spectrum is ergodic, see Fig. 1(c), like in the

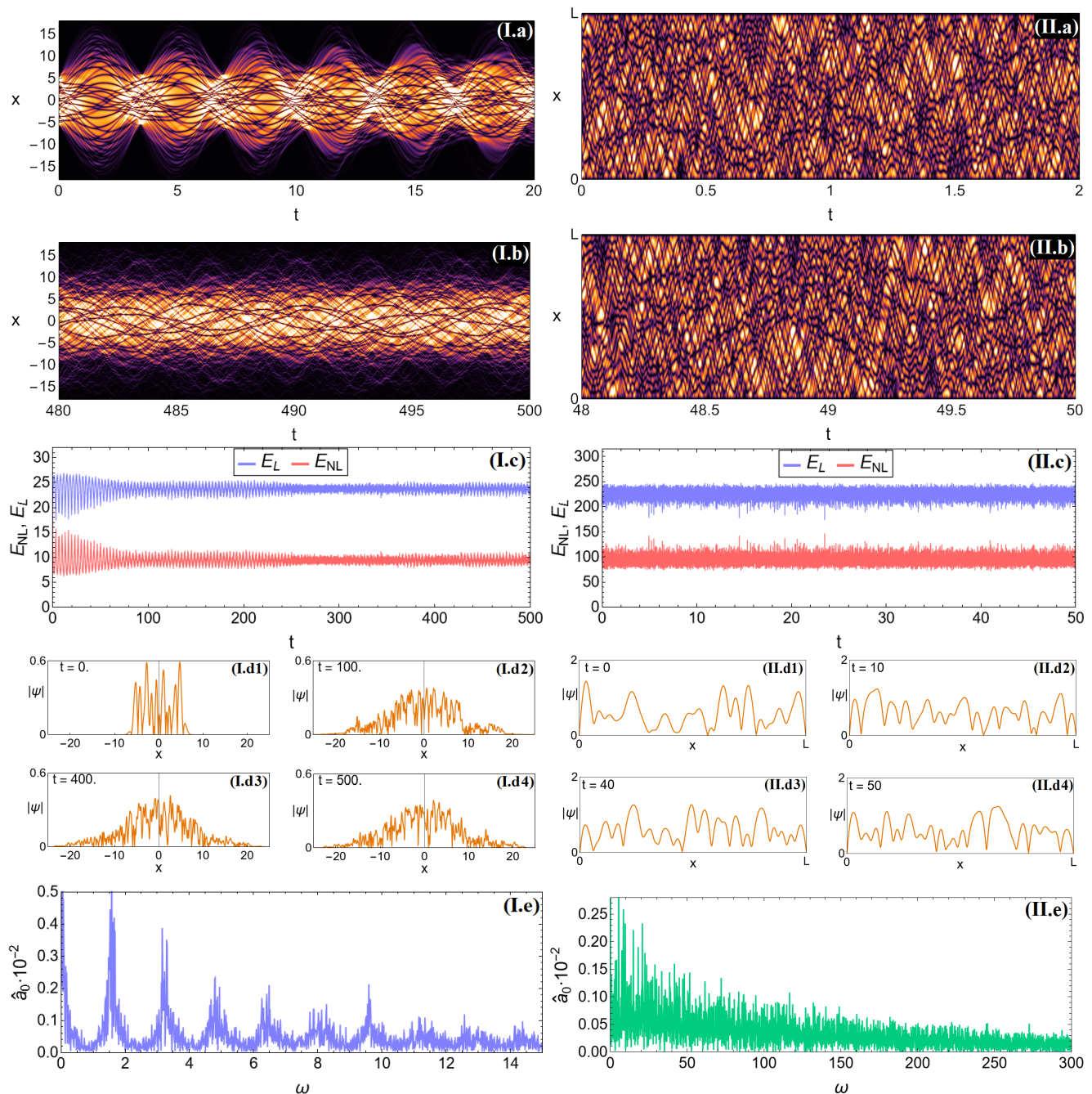


FIG. 2. The evolution of 1D defocusing random waves under the action of the HO (left column, labeled I) or box of size $L = \pi/\sqrt{2}$ (right column, labeled II), for a large nonlinearity coefficient $g = 250$ in Eq. (2). From top to bottom: the initial stage of the spatiotemporal evolution (a); the evolution at an advanced stage (b); the temporal evolution of the quadratic (5) and quartic (6) energies (c); four snap-shots illustrating the shape of the condensates in the course of the evolution (d); and the power spectrum of the lowest-mode's amplitude, $\alpha_0(t)$, (e), with higher modes displaying similar shapes. The initial conditions are random waves prepared as per Eq. (12) with $\mathcal{N} = 20$ and $\beta = 1$. Both cases corresponding to the HO and box potentials keep $H_4/H_2 \simeq 0.42$ most of the time.

case of the box potential, see Fig. 2II.e, in agreement with the general picture outlined above.

III. ANALYTICAL DESCRIPTION IN THE WEAKLY NONLINEAR REGIME

In this section, we aim to provide an analytical form of the power spectrum in the weakly nonlinear regime,

$|g| \ll 1$ in Eq. (2), where the difference in the emergence of comb-like or ergodic spectra in HRP and non-HRP can be understood explicitly. To do that, we again address the 1D GPE with the HO and box potentials, which generate, as mentioned above, the following commonly known equidistant and quadratic spectra:

$$\mathbf{HO}: E_n = n + \frac{1}{2}; \quad \mathbf{box}: E_n = \frac{\pi^2}{2L^2}(n+1)^2. \quad (14)$$

First, we are going to demonstrate that both potentials produce, in the case of extremely weak nonlinearity, a comb-like power spectrum composed of “slender” peaks. After that, we show how the eigenvalues determine interactions between the eigenmodes, and how the equidistant eigenvalues in the case of the HO potential arrange the interactions in a way that helps with preserving the comb-like spectrum when the nonlinearity strengthens. On the other hand, we will see that the deviation from the equidistant structure of the spectrum in the case of the box potential is responsible for erasing the comb-like spectral shape, already at moderately weak coupling. The extension of the analysis to generic HRP subject to condition (1) is presented in Appendix B. We show there that our arguments developed for the HO potential apply to generic HRP as well, safeguarding the preservation of the comb-like power spectra. The arguments are independent of the sign of g , being valid for both the defocusing and focusing signs of the nonlinearity. For this reason, g will mean $|g|$ in this section.

A slender comb-like spectrum

For our analysis, it is useful to rewrite the 1D GPE (2) as a system of equations for mode amplitudes α_n . To do that, one has to insert $\psi(t, x)$, written in the form of expansion (10), in Eq. (2), and project the result onto eigenmodes $f_n(x)$. This results in a system of ordinary differential equations for the evolution of the amplitudes,

$$i \frac{d\alpha_n}{dt} = g \sum_{m=0}^{\infty} \sum_{i=0}^{\infty} \sum_{j=0}^{\infty} C_{nmij} \bar{\alpha}_m \alpha_i \alpha_j e^{i\Delta_{nmij}t}, \quad (15)$$

where the bar denotes complex conjugation,

$$\Delta_{nmij} = E_n + E_m - E_i - E_j \quad (16)$$

are the resulting frequencies of the four-wave interaction, and couplings constants of the interactions are

$$C_{nmij} = \int_{-\infty}^{+\infty} f_n(x) f_m(x) f_i(x) f_j(x) dx. \quad (17)$$

Expressions (15)-(17) are valid for any trapping potential, including the HO and box ones, the distinction being in the values of Δ_{nmij} and C_{nmij} , when one inserts specific eigenvalues E_n and eigenmodes $f_n(x)$ into the expressions.

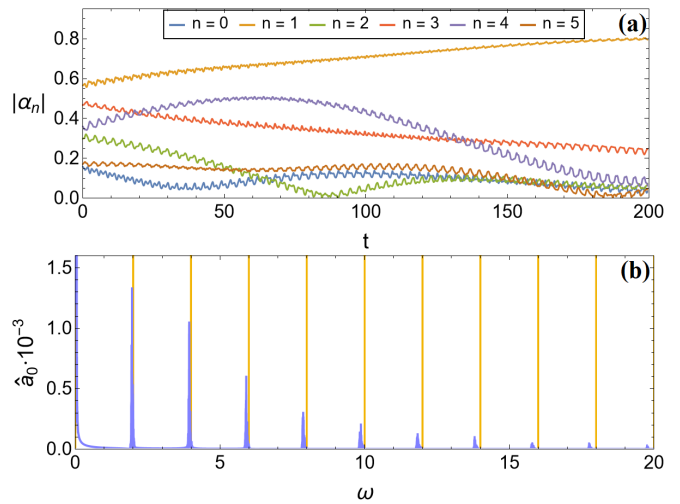


FIG. 3. The evolution of α_n (a) and power spectrum of $|\alpha_0|^2$ (b) governed by the defocusing 1D GPE with the HO potential. In (a) two constituents of the evolution are observed: long-time modulations and small-amplitude oscillations, which are associated with resonant and non-resonant interactions, respectively. In (b) the effect of these terms on the power spectrum of $|\alpha_0|^2$ is observed. Vertical yellow lines mark our analytic prediction, $\mathcal{W}_{2k} = 2k$, for the location of the excited frequencies in the case of the weak nonlinearity [see Eq. (19)], which demonstrates very accurate agreement, up to a slight shift originating from nonlinear corrections. These numerical results were produced for $g = 1$, to be able to comprise the slow and fast constituents in the evolution of α_n in the framework of the same plot. This illustrates that the analytical prediction obtained for $g \ll 1$ works very well in this case too.

Using Eqs. (15), we aim to demonstrate, first, that the structure of the power spectrum is quite simple for the weak nonlinearity ($g \ll 1$). The equations give rise to two constituents of the evolution, as seen in Fig. 3. On the one hand, there are frequencies $\sim g$ and amplitudes ~ 1 , which are associated with resonances ($\Delta_{nmij} = 0$). On the other hand, there are contributions of small amplitude $\sim g$ corresponding to frequencies associated with non-resonant interactions ($\Delta_{nmij} \neq 0$). This latter class of frequencies are precursors of the characteristic spikes in the comb-like spectrum which exist in the case of strong nonlinearity, as shown in the next section. In view of their relevance to the analysis, we introduce them by means of the following definition.

Definition: \mathcal{W}_k with $k \in \mathbb{Z}$ corresponds to all different values taken by Δ_{nmij} with $n, m, i, j \in \mathbb{N}$, defined by Eq. (16) arranged in the increasing order,

$$\dots < \mathcal{W}_{k-1} < \mathcal{W}_k < \mathcal{W}_{k+1} < \dots \quad \text{with } k \in \mathbb{Z}. \quad (18)$$

When Δ_{nmij} takes the same value for different sets of the indices, there is single \mathcal{W}_k associated with that value. (For instance, $\Delta_{nnnn} = 0$ for any n , hence there is single k for which $\mathcal{W}_k = 0$.)

For generic systems, eigenvalues E_n are irrational numbers, hence \mathcal{W}_k will form a rather dense set on the real

line (denser than the set of E_n themselves). As one proceeds to stronger nonlinearity, further combinational harmonics will arise, filling in the real line still more densely, and leading to the emergence of generic continuous power spectra. The situation is much more subtle for systems with integer eigenvalues E_n , as is the case for the HO and box potentials, since \mathcal{W}_k are then integers too. In this case, further analysis is required to identify the shape of the power spectra.

The structure of the power spectra arises from the effect of the right-hand side (RHS) of (15) on the evolution of α_n . In this context, two key ingredients are the prefactor g , and the complex exponential, which is an oscillatory term with frequency Δ_{nmij} that vanishes in the resonant case, $\Delta_{nmij} = 0$. When g is very small, the evolution splits into components corresponding to the natural time scales, $t \sim \mathcal{O}(1)$, $\mathcal{O}(1/g)$, etc. [80, 81]. For $t \sim \mathcal{O}(1)$, α_n remain constant up to nonlinear contributions of orders $\sim g$ and higher. We focus on the ones of order g because they dominate in this regime. On the one hand, resonant terms with $\Delta_{nmij} = 0$ generate contributions $\sim gt$ (i.e., secular terms in terms of the “naive expansion” in powers of g), which induce substantial modulations in α_n at times $t \sim \mathcal{O}(1/g)$, (see the slow evolution of $|\alpha(t)|$ in Fig. 3). Therefore, such long-time modulations excite frequencies $\sim g$ in the power spectrum. On the other hand, non-resonant terms, with $\Delta_{nmij} \neq 0$, oscillate with frequencies Δ_{nmij} (including corrections $\sim g$) and amplitudes $\sim g$ (see small oscillations of $|\alpha(t)|$ in Fig. 3). The latter terms excite frequencies Δ_{nmij} in the power spectrum of α_n (with corrections $\sim g$), and have amplitudes $\sim g$. From here, we conclude that the structure of the power spectrum in the weakly nonlinear regime includes two kinds of excitation frequencies: the ones determined by \mathcal{W}_k , and the frequencies forming a continuum in a small region of width $\sim g$ around the origin. When the nonlinearity strength grows, frequencies produced as combinations from these two sets will emerge, being responsible for the broadening of the sharp peaks located at various values of \mathcal{W}_k .

From the previous discussion, one can deduce the condition to display the comb-like power spectrum in the regime of weak nonlinearity. This is just the condition that \mathcal{W}_k must be equidistant because the spectrum is tightly localized around \mathcal{W}_k . The 1D GPE with the HO and box potentials precisely satisfy this property because they give rise to

$$\mathcal{W}_{2k} = 2k \quad (19)$$

and $\mathcal{W}_{2k} = \pi^2 k/L^2$, respectively. This means that both potentials give rise a “slender” version of the comb-like power spectrum at extremely weak nonlinearity. The expressions for \mathcal{W}_{2k} follow from Eqs. (14) and (16)

$$\Delta_{nmij} = (n + m - i - j) \quad \text{with} \quad n, m, i, j \in \mathbb{N}, \quad (20)$$

$$\Delta_{nmij} = \frac{\pi^2}{2L^2} [(n+1)^2 + (m+1)^2 - (i+1)^2 - (j+1)^2], \quad (21)$$

in the case of the HO and box potential, respectively. To make the structure of expression (21) more transparent, we set $m = i - 1$, $j = n - 1$, which yields $\Delta_{nmij} = \pi^2(n - i)/L^2$, so that any integer is generated (times π^2/L^2). We use index $2k$, instead of k , to highlight the absence of interactions between three modes with odd numbers and an even one, and vice versa, for parity reasons (the respective couplings C_{nmij} vanish according to Eq. (17), hence \mathcal{W}_{2k+1} are not present in the power spectrum). To ensure a meaningful comparison between the HO and box potentials, we choose, as said above, $L = \pi/\sqrt{2}$. Then, the spike positions (\mathcal{W}_{2k}) in the power spectrum are the same for the two cases in the weakly nonlinear regime. By means of such identification of the frequency scales, a meaningful comparison is possible between the HO and box potentials, also for strong nonlinearity.

Departing from the weakly nonlinear regime

It has been demonstrated above that the 1D GPE with the HO or box potentials display a comb-like power spectrum for extremely weak nonlinearity. However, as Figs. 1 and 2 show, this shape of the spectrum is not preserved in the case of the box potential, which turns into a generic ergodic spectrum with the increase of the nonlinearity strength. We are going to explain why, on the other hand, the HO potential preserves the comb-like shape of the power spectrum even at strong nonlinearity. We will demonstrate that the key difference is the linear and quadratic eigenvalue spectra (14) of these systems. This is because the eigenvalues determine, through the frequency combinations Δ_{nmij} , which modes are involved in the four-wave interactions, and then different structures of Δ_{nmij} in Eqs. (20) and (21) produce different predictions for the excitation of frequencies \mathcal{W}_k . We will show that, through this mechanism, equidistant eigenvalues produce a strong suppression of large frequencies, while a large range of them get excited in case of the quadratic eigenvalue spectrum in Eq. (14). To show this, one has to estimate the contribution of the k -th frequency \mathcal{W}_k to the n -th mode α_n . For that purpose, one gathers all terms oscillating with frequency \mathcal{W}_k on the RHS of (15), writing the system of equations in the form

$$i \frac{d\alpha_n}{dt} = g \sum_{k=-\infty}^{\infty} \mathcal{S}_n(k) e^{i\mathcal{W}_k t}, \quad (22)$$

$$\mathcal{S}_n(k) \equiv \underbrace{\sum_{m=0}^{\infty} \sum_{i=0}^{\infty} \sum_{j=0}^{\infty} C_{nmij} \bar{\alpha}_m \alpha_i \alpha_j}_{\Delta_{nmij} = \mathcal{W}_k}. \quad (23)$$

The “sources” $\mathcal{S}_n(k)$ defined by Eq. (23) determine the contribution of the k -th frequency \mathcal{W}_k to the n -th mode α_n . Numerical computations using values of α_n extracted

from our simulations reveal that $\mathcal{S}_n(k)$ decay with $|k|$ considerably faster for the HO potential than the box potential, as Fig. 4 illustrates. This picture is confirmed analytically in Appendix B showing that the amplitudes $\mathcal{S}_n(k)$ decay exponentially in the former case,

$$|\mathcal{S}_n(|k| \gg n)_{\text{HO}}| < e^{-\beta|k|} P_{n,k}, \quad (24)$$

while they exhibit a much slower decay in the latter one,

$$|\mathcal{S}_n(|k| \gg n^2)_{\text{box}}| < e^{-\beta\sqrt{|k|}} D_{n,k}, \quad (25)$$

where, $P_{n,k}$ and $D_{n,k}$ are polynomials in n and k , and β is a positive constant. To derive these results, we have used a “phenomenological” analytical expression for α_n that captures the qualitative structure revealed by our simulations, see Fig. 4(c),

$$|\alpha_n| < p_n^{(s)} e^{-\beta n} \mathcal{A}_n, \quad (26)$$

where $\beta > 0$ is the same constant as in Eqs. (24) and (25), $p_n^{(s)}$ is a polynomial of degree $s \geq 0$, while \mathcal{A}_n is a random variable uniformly distributed on $[0, 1]$.

Below, we explain that the difference between the HO and box potentials in the decay of $|\mathcal{S}_n(k)|$ with k has an impact on the structure of the power spectrum in the cases of weak and moderate nonlinearities, but, before that, we should clarify where this difference comes from. One might conjecture that it is associated with the couplings C_{nmij} , but the actual reason is the difference between the equidistant (8) and quadratic (9) energy spectra, together with the rapid decay of α_n (26). As we show in Appendix B, for HRP’s satisfying condition (1), such as the HO potential, and α_n given by (26), $\mathcal{S}_n(k)$ decays exponentially for large $|k|$, independent of whether C_{nmij} decay, remain constant, or grow with the increase of the indices, while systems with quadratic spectrum, such as the one corresponding to the box potential, feature a much slower decay. The key point is in the restriction on the indices necessary to get $\Delta_{nmij} = \mathcal{W}_k$ in Eq. (23). Namely, fixing k , the modes involved in the interactions that generate frequency \mathcal{W}_k differ between the spectra (20) and (21). In the former case, large k requires at least one high-order mode involved, while in the latter case the quadratic eigenvalues make it possible to achieve large k using low-order modes. Thus, the exponential decay of high modes gives rise to the difference in the magnitude of $\mathcal{S}_n(k)$. The following example illustrates this picture.

Example: Frequency \mathcal{W}_{45} contributes to α_5 via several combinations of modes $\{n, m, i, j\}$ in (23). For the sake of simplicity we use the following expressions in this example:

$$\alpha_n = e^{-n}, \quad \text{and} \quad C_{nmij} = 1, \quad (27)$$

while the conclusion is the same for other choices of α_n and C_{nmij} , as explained in Appendix B. We look for one of the largest contributions to $\mathcal{S}_5(45)$, which is the one

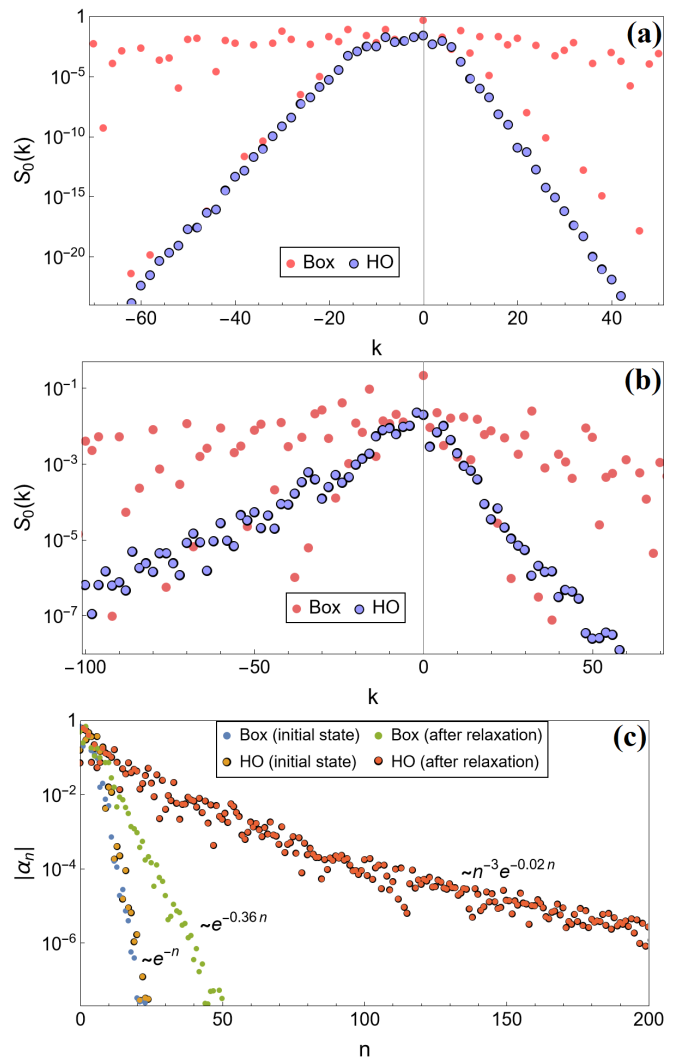


FIG. 4. The dependence of amplitude $\mathcal{S}_0(k)$ on k in the cases of the HO and box potentials, as produced by the numerical solutions initialized by input (12) with the random phase and amplitude, for $\mathcal{N} = 5$ and $\beta = 1$. Plot (a) shows $\mathcal{S}_0(k)$ associated with the initial state, namely, when α_n feature the exponential decay e^{-n} in both systems. Plot (b) shows the same amplitudes after the relaxation of the systems, when α_n demonstrate a stronger suppression with n in the box ($\sim e^{-0.36n}$) than in the HO ($\sim n^{-3}e^{-0.02n}$), while $\mathcal{S}_0(k)$ still decay faster in the latter case. Plot (c) shows the values of $|\alpha_n|$ used in (a) and (b).

involving the lowest possible modes, $\{5, 40, 0, 0\}$ in the case of the HO spectrum (20), or $\{5, 2, 0, 0\}$ in the case of the box spectrum (21). Then, it follows from Eq. (23) that the contribution of this interaction in the case of the HO potential, $\bar{\alpha}_{40}\alpha_0\alpha_0 = e^{-40}$, is many orders of magnitude smaller than the one in the case of the box potential, $\bar{\alpha}_2\alpha_0\alpha_0 = e^{-2}$, because they, respectively, involve modes $m = 40$ and $m = 2$ to generate the same frequency \mathcal{W}_k .

At weak nonlinearity, the difference in the decay of amplitudes $\mathcal{S}_n(k)$ corresponding to the HO and box po-

tentials has an impact on the power spectrum because they determine the excitation of frequencies \mathcal{W}_k . The strong suppression of $\mathcal{S}_n(k)$ in the HO case is translated into strong suppression of high frequencies \mathcal{W}_k (rapid decay of peaks in the comb-like power spectrum), while the much slower suppression of $\mathcal{S}_n(k)$ in the case of the box potential facilitates excitation of higher frequencies (the presence of spectral peaks at higher frequencies). In the regime of moderate nonlinearity, amplitudes $\mathcal{S}_n(k)$ have an even stronger influence on the shape of the power spectrum, as we aim to explain now. In this regime, the evolution of α_n no longer consists solely of two motions contributed to by resonances ($\Delta_{nmij} = 0$) and oscillations with frequencies \mathcal{W}_k , like in Fig. 3(a), but subdominant oscillatory terms start to become relevant. Thereby, the equidistant structure of \mathcal{W}_k is no longer sufficient to maintain the comb-like spectrum. Subdominant components emerge from the combination of the resonant and non-resonant terms, as mentioned above. Namely, these combined terms act as sources driving the generation of subdominant components (similar to the usual principle that, in any perturbative expansion, higher-order terms are sourced by lower-order ones). The terms that emerge have frequencies resulting from combinations of \mathcal{W}_k and the ones of order g around the origin. They produce contributions in the power spectrum that slightly deviate from \mathcal{W}_k broadening in this way the “slender” spikes in the power spectrum in the regime of weak nonlinearity. This set of subdominant contributions is naturally extended at higher orders in g , producing more and more frequencies in the power spectrum which are originally sourced by $\mathcal{S}_n(k)$. Therefore, the behavior of these amplitudes determines how the power spectrum is populated when a system departs from the weakly nonlinear regime. In the case of the box potential, we have demonstrated above that $\mathcal{S}_n(k)$ slowly decay with $|k|$ [see Eq. (25)], thus giving rise to a broad range of high frequencies \mathcal{W}_k , and thus triggering the rise of a large number of high-frequency subdominant peaks, which dress the basic power spectrum with a complicated structure. In this way, the comb-like spectral shape, which exists in the weakly nonlinear regime, quickly gets destroyed, a spectral tail of high frequencies arises, and individual peaks broaden considerably, absorbing multiple combinational contributions arising from already excited peaks. In the case of the HO potential, higher-order contributions are of course produced as well, but the exponential suppression of high-frequencies \mathcal{W}_k , seen in Eq. (24), ensures that a majority of subdominant terms are suppressed as well. This mechanism drastically reduces the number of significant subdominant contributions the power spectrum receives, preventing its “wild” population and protecting its comb-like structure. Note that, while our analysis is performed within the weakly nonlinear regime, the picture produced by it correctly captures the shapes of the power spectra for strong nonlinearity, as observed in Figs. 1 and 2: a disordered distribution of many spikes in the case of the box potential, and the nearly equidis-

tant array of spikes in the HO case, confined to the low-frequency range.

IV. NUMERICAL RESULTS IN THE FULLY NONLINEAR REGIME

Having explained the emergence of comb-like power spectra at weak nonlinearity, it is natural to explore how the picture changes towards strong nonlinearity. Specifically, it is relevant to find out how the structure gradually deviates from the above prediction for the weakly nonlinear regime, i.e., its behavior for large $|g|$, and how it depends on the sign of the nonlinearity, self-defocusing ($g > 0$) or focusing ($g < 0$).

Figure 5 provides answers to these questions. One observes how the comb-like spectrum evolves away from the “slender” version as the nonlinearity strength grows, for the 1D GPEs with the box and HO potentials. The comparison between these potentials demonstrates how the main predictions of the weakly nonlinear analysis developed above still hold qualitatively in the fully nonlinear regime. The power spectrum for the box potential transits from the comb-like shape to an ergodic one, which includes a conspicuous high-frequency component for large g . Nevertheless, the spectrum corresponding to the HO potential still keeps a comb-like spectral shape for large values of $|g|$. This contrast between the different potentials reflects the fact that the equidistant linear energy spectrum (1) plays a central role in the nonlinear regime too. It is relevant to stress that these results are not explained by proximity to the linear regime. Indeed, in both cases of the HO and box potentials, the “slender” power spectra exist close to the linear limit (small g). However, extending them to a comparable level of the dynamical nonlinearity characterized by the ratio H_4/H_2 of the energy terms, see Eqs. (5) and (6), the GPE with the HO potential still displays a comb-like spectrum, while its counterpart with the box potential displays an ergodic spectrum, totally deviating from the quasi-linear behavior.

For the case of the HO potential in the GPE with focusing and defocusing nonlinearities, Fig. 5 shows two characteristic effects involving spikes of the comb-like spectra. The first is a gradual deviation from locations \mathcal{W}_k predicted in the weak-nonlinearity regime, towards smaller (larger) frequencies for the defocusing (focusing) sign of the nonlinearity, while keeping their nearly-equidistant structure. The second effect, observed with the growth of $|g|$, is that the spectral spikes get wider, and at some point they start to overlap with each other, compromising the comb-like shape. The magnitude of $|g|$ at which this happens depends on the sign of the nonlinearity. In the case of the self-attraction, the transition happens at much lower values of $|g|$.

Note that the above analysis is presented for the nonlinearity magnitude, g , treated as the control parameter. An alternative way to quantify the strength of the

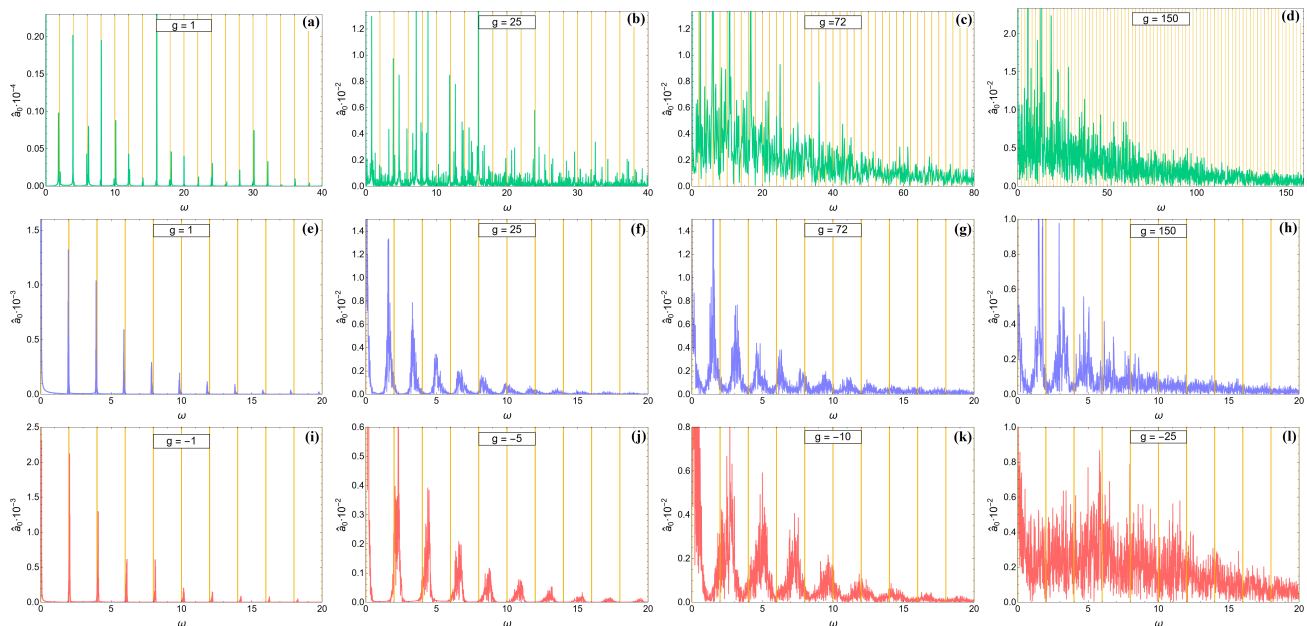


FIG. 5. The power spectrum produced by the defocusing 1D GPE with the box potential (a)-(d), and by the defocusing and focusing ((e)-(h) and (i)-(l), respectively) 1D GPE with the HO potential. The computations of the spectra for increasing values of the nonlinearity strength, $|g|$, are performed with random-wave initial conditions. The initial data are the same for all plots in the case HO case. Vertical yellow lines mark the location of \mathcal{W}_{2k} , see Eq. (19).

nonlinearity is, as mentioned above, to use the ratio between the quadratic and quartic energies, $|H_4|/H_2$. We observe that, with $|g|$ increasing, the self-focusing GPE rapidly accumulates energy in the nonlinear terms, which is translated into larger values of $|H_4|/H_2$, in comparison to the defocusing case, which requires much higher values of g to reach the same ratio.

The transition from the comb-like power spectrum to ergodicity in the case of very strong nonlinearity is not surprising. What is nontrivial in these results, is the great impact the equidistant structure of the spectrum of linear eigenvalues on the nonlinear regime and the persistence of non-ergodic spectra even at strong nonlinearity.

V. OTHER NLSES WITH HRPS (HIGHLY-RESONANT POTENTIALS)

In the above analysis, we have been using the 1D GPE with the HO potential as the guiding example to present the characteristic features of HRPs and observe how their resonances hinder the onset of the ergodicity. In this section, we proceed to demonstrate that this effect is generic for other resonant potentials, which in fact cover a wide range of interesting models. To this end, we have explored the dynamics of NLSEs with different nonlinearities, including HRPs in different spatial dimensions, a two-component NLSE, and even a related relativistic wave equation. Below, we present detailed results for these equations. In Fig. 6, one can see that all of them display comb-like power spectra, confirming the generic-

ity of the principles formulated above. Actually, these findings imply that the form of the nonlinearities plays a secondary role, as it determines the values of g at which comb-like spectra transit to ergodic ones, but not the overall presence of the effect.

1) The quintic 1D NLSEs with the HO potential: A natural modification of the original 1D GPE with the HO potential is to replace the cubic nonlinear term by the quintic one. The equation has the form

$$i\partial_t\psi = -\frac{1}{2}\partial_{xx}\psi + \frac{1}{2}x^2\psi + g|\psi|^4\psi, \quad (28)$$

keeping the equidistant spectrum, $E_n = n + 1/2$. This modification provides a new setting because the cubic 1D NLSE in the free space is integrable, while the quintic one is not, and gives rise to 1D Townes solitons and critical collapse [82]. This, in particular, rules out the integrability of the underlying equation in the free space as a reason for the emergence of comb-like power spectra.

2) D-dimensional cubic and quintic NLSEs with the HO potential: It is also natural to explore the existence of comb-like power spectra in higher dimensions (here we restrict the consideration to the case of spherical symmetry). We did that for the cubic and quintic NLSEs with the HO potential:

$$i\partial_t\psi = \frac{1}{2}\left(-\partial_{rr} - \frac{D-1}{r}\partial_r + r^2\right)\psi + g|\psi|^{p-1}\psi, \quad (29)$$

where $r \in [0, \infty)$ is the radial coordinate, $D = 2, 3, \dots$ is the spatial dimension, and $p = 3$ or 5 is the power of the nonlinear term. For any combination of these parameters

and $g > 0$ (self-repulsion, otherwise the multidimensional NLSE gives rise to the collapse [83]), Eq. (29) has the commonly known equidistant linear energy spectrum of the multidimensional HO, $E_n = 2n + d/2$.

3) Anharmonic potentials: Another way to test the robustness of our findings is by modification of the trapping potential, keeping its equidistant spectral structure. Some special 1D potentials which maintain this property can be found in Ref. [84]:

$$V^{(1)}(x) = \frac{x^2}{2} + \frac{s^2 - 1}{8x^2}, \quad (30)$$

$$V^{(2)}(x) = \frac{x^2}{2} + \frac{3}{x^2} \frac{4x^4 + 3}{(2x^2 + 3)^2} + \frac{4}{3}, \quad (31)$$

$$V^{(3)}(x) = \frac{x^2}{2} + \frac{8x^2 - 4}{(2x^2 + 1)^2} + \frac{2}{3}, \quad (32)$$

$$V^{(4)}(x) = \frac{x^2}{2} + 8 \frac{(8x^6 + 12x^4 + 18x^2 - 9)}{(4x^4 + 12x^2 + 3)^2} + 2, \quad (33)$$

where $s > 1$ is a constant, $x \in (0, \infty)$ for the first two potentials, and $x \in (-\infty, \infty)$ for the last two. The energy eigenvalues are fully equidistant for $V^{(1)}$ and $V^{(2)}$,

$$E_n^{(1)} = 2n + 1 + \frac{s}{2}, \quad E_n^{(2)} = 2n + \frac{23}{6}, \quad (34)$$

with $n \geq 0$, while for $V^{(3)}$ and $V^{(4)}$ there is a gap between the ground-state eigenvalue and ones corresponding to the excited states, which form equidistant arrays (“towers”):

$$E_0^{(3)} = -\frac{5}{6}, \quad E_{n \geq 1}^{(3)} = n + \frac{7}{6}, \quad (35)$$

$$E_0^{(4)} = -\frac{3}{2}, \quad E_{n \geq 1}^{(4)} = n + \frac{5}{2}. \quad (36)$$

The dynamics produced by the 1D GPE with potential $V^{(1)}$, given by Eq. (30), is identical to the D-dimensional NLSE with the HO potential and nonlinear term $r^{D-1}|\psi|^2\psi$ (see appendix C for the derivation), but, in any case, the equation is different from (2) or (29).

4) A two-component NLSE system: Another possibility [55, 85–88] to realize the comb-like (non-ergodic) power spectra is offered by a two-component 1D NLSE,

$$\begin{cases} i\partial_t u = -\frac{1}{2}\partial_{xx}u + \frac{x^2}{2}u + cv + g_u|u|^2u, \\ i\partial_t v = -\frac{1}{2}\partial_{xx}v + \frac{x^2}{2}v + cu + g_v|v|^2v, \end{cases} \quad (37)$$

where g_u , g_v and c are constants. The linear version of the system can be decoupled in two single-component equations for $\psi_+ = u + v$ and $\psi_- = u - v$, which gives rise to two “towers” of equidistant energy eigenvalues, $E_n^{(\pm)} = n + \frac{1}{2} \pm c$.

5) A wave equation in anti-de Sitter spacetime: Our considerations of the comb-like spectra are based on the equidistant energy spectrum (1), and depend little on peculiarities of the NLSEs. We have further tested the validity of the principles formulated here for the case

of a relativistic wave equation whose normal-mode frequencies also fit (1). This choice is motivated by the connection between the GPE and the following equation for a real scalar field ϕ in the anti-de Sitter spacetime [83, 89, 90]:

$$\partial_{tt}\phi = \cot^2 x \partial_x(\tan^2 x \partial_x\phi) + g\phi^3, \quad (38)$$

which is subject to boundary condition $\phi(t, \pi/2) = 0$, where $x \in [0, \pi/2)$ is the radial coordinate. This equation gives rise to an equidistant spectrum, $E_n = 2n + 3$.

VI. DISCUSSION

Our analysis has revealed that NLSEs with HRP (highly resonant potentials) pose a barrier to the emergence of ergodic power spectra even as one progresses to the fully nonlinear regime. While usually the consideration of non-ergodic dynamics is restricted to small deformations of integrable equations [7–11, 14–17, 21–23], our focus has been on mechanisms that do not directly rely on proximity to integrability. The potentials in question, namely, the ones with equidistant linear spectra of energy eigenvalues, in particular, the HO (harmonic-oscillator) potential, produce a strong impact on the power spectra, which remain concentrated in comb-like arrays of spikes. This pattern is captured by both our analytic consideration for weak nonlinearity, performed in Section III, and numerical simulations of the strongly nonlinear regime in Section IV. These spectra are in clear contrast with the continuous ones produced by generic potentials, and resemble quasi-discrete spectra associated with integrable dynamics.

While the difference between the HRP and generic potentials without any resonances is obvious, the difference is more subtle when comparing HRP to potentials that feature some resonances in their spectra, but the energy levels do not fit the rigid pattern defined by Eq. (1). In the case of generic potentials, normal-mode frequencies are incommensurate, and combinational frequencies created by nonlinearities quickly populate the real line, creating a generic continuum power spectrum. For that reason, much of our study has been focused on the peculiar but physically motivated case of the infinitely deep box potential. In that case, the linear normal-mode frequencies and all of their combinations are integers, which, however, does not preclude the emergence of the continuum power spectrum at finite nonlinearity strength, in contrast to what is seen in the case of the HO harmonic potential and other HRP with linear energy spectra in the form of Eq. (1). The analytical consideration of the weak-nonlinearity regime, carried out in Section III, makes it clear that the central role is played by the spectrum of linear energy eigenvalues. They determine the interactions between the modes in the system, which translates into the structure of the power spectrum. Equidistant energy eigenvalues, like those in the case of the HO potential, distribute the interactions in such a special way

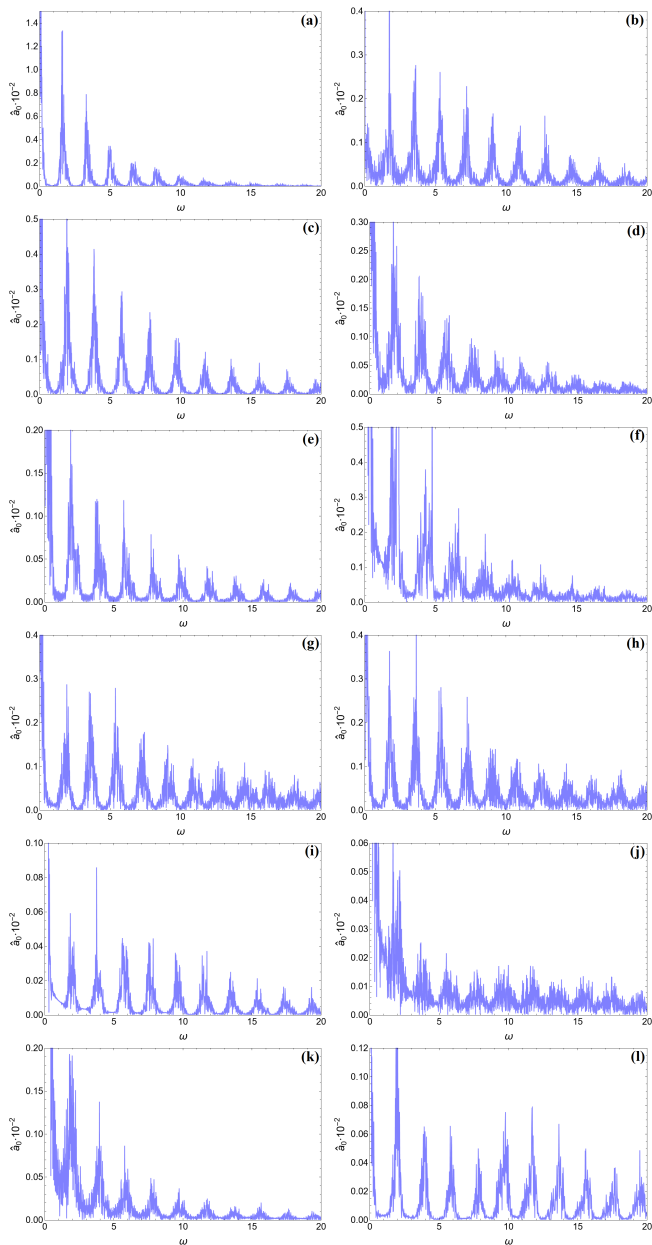


FIG. 6. Comb-like power spectra produced by the 1D, 2D, and 3D GPEs (a-c), by the 1D, 2D, and 3D quintic NLSEs with the HO potential (d-f), by the 1D NLSE with potentials $V^{(1)}$, $V^{(2)}$, $V^{(3)}$, $V^{(4)}$ defined by Eqs. (30) – (30) [panels (g-j), respectively], by the two-component NLSE (37) (k), and by the relativistic real wave equation (38) (l).

that a reduced set of frequencies dominate in the power spectrum, providing, in particular, strong suppression of high frequencies and ensuring the protection of the non-ergodic comb-like power spectra in the regime of stronger nonlinearity. On the other hand, the quadratic energy eigenvalues produced by the box potential do not provide for the suppression of higher frequencies, and give rise to truly continuous ergodic spectra. This analysis is extended to a broad class of HRPs in Appendix B,

leading to the same conclusion. Further, we have made use of simulations to study the dependence of the comb-like power spectrum on the nonlinearity strength, and tested the genericity of our conclusions, checking them for NLSEs with various HRPs. Random waves were used as the initial conditions to capture the evolution of a wide range of initial configurations. Our numerical results give evidence that the analysis developed in the weak-nonlinearity limit correctly forecasts the qualitative shape of the power spectra in the strongly nonlinear regime as well. We also inspected the distinction between the cases of focusing and defocusing nonlinearities, concluding that the comb-like power spectra degrade faster with the growth of the nonlinearity strength in the former case.

In general, linear features tend to get rapidly overwhelmed by nonlinear effects when the system departs from the weakly nonlinear regime, although some models for 1D random waves demonstrate regimes where dynamical features of the weak and full nonlinearities coexist [91] (i.e., random waves and coherent modes, such as solitons, exist simultaneously). HRPs admit similar coexistence between the features of weak nonlinearity and fully nonlinear dynamics: while solitons (and other essentially nonlinear effects) are involved in the dynamics, it is still heavily influenced by the weak-nonlinearity features, such as the structure of the spectrum of energy eigenvalues. As a result, the comb-like power spectra, which are directly associated with weakly nonlinear dynamics, persist for stronger nonlinearity.

After producing the basic results with the help of the guiding example of the 1D GPE with the HO potential, we have demonstrated that the same mechanism of the obstruction to ergodicity is maintained by generic HRPs. To do that, in addition to the analytical description developed in Section III and Appendix B, we have explored several NLSEs in this class of potentials. We observed comb-like power spectra in the presence of different nonlinear terms, different potentials (belonging to the HRP class), different spatial dimensions, and in the two-component GPE as well. The presence of the multidimensional models in the class of highly resonant NLSEs, such as the 2D and 3D GPEs and quintic NLSE with the HO potential is a noteworthy finding. This is in contrast to studies to non-ergodic dynamics that rely on proximity to integrability, as a vast majority of integrable equations are one-dimensional. In this work, we have studied the obstruction to ergodicity in the multidimensional equations under the assumption of spherical symmetry. It would be interesting to lift this condition, addressing fully multidimensional spectra.

Our study suggests an extension of the concept of quasi-integrability, observed in the form of quasi-discrete power spectra in the 1D GPE with the HO potential and self-defocusing cubic nonlinearity [46]. The case of self-focusing remained unexplored until now. We have tackled it here too, demonstrating the presence of the comb-like power spectra in this case as well, although

they degrade faster with the growth of the nonlinearity strength. We have provided an analytical description of this effect at the regime of weak nonlinearity, while previously reported results were purely numerical. Finally, we have broadened the understanding of quasi-integrability by showing that its characteristic quasi-discrete power spectrum, produced by the evolution of random-wave initial conditions, is shared by a large class of HRPs (highly resonant potentials). Thus, our results imply that the 1D GPE with the HO potential is not exceptional in this regard, although it is worthwhile to mention the large range of the strength of the defocusing nonlinearity for which this physically relevant model produces well-defined comb-like power spectra. While we have mostly focused on NLSEs, our weakly nonlinear analytics suggests that the obstruction-to-ergodicity mechanism should be present in equations of other types, such as nonlinear wave equations. We have briefly demonstrated the latter possibility by presenting the comb-like power spectrum generated by the highly-resonant real wave equation (38).

ACKNOWLEDGMENTS

AB thanks Z. Hani, G. Staffilani, and J. Amette, for useful discussions. In the course of this work AB has been supported by the Polish National Science Centre grant No. 2017/26/A/ST2/00530 and by the LabEx ENS-ICFP: ANR-10-LABX-0010/ANR-10-IDEX-0001-02 PSL*. OE has been supported by Thailand NSRF via PMU-B (grant numbers B01F650006 and B05F650021) and by FWO-Vlaanderen through project G006918N. BAM has been supported, in part, by the Israel Science Foundation (grant No. 1695/22).

Appendix A: Numerical methods

Numerical simulations of NLSEs have been performed using two schemes. One is based on a pseudo-spectral decomposition of the spatial coordinate similar to that used in Refs. [73, 76, 92] and the fourth-order Runge-Kutta (4RK) method to advance in time. When the spatial coordinate is unbounded, $x \in (-\infty, \infty)$, such as in the case of the 1D GPE with the HO potential, we truncate the domain to a finite one $x \in [-R_{\max}, R_{\max}]$ with R_{\max} large enough to guarantee that $|\psi(t, \pm R_{\max})|$ is exponentially suppressed. This interval is discretized into N points of the form $x_n = R_{\max}(\frac{2n}{N} - 1)$ with $n = 0, 1, \dots, N-1$. The goal of this procedure is to compute the second derivative on the RHS of the equation by using the Fast Fourier transform (FFT). For this purpose, we decompose function $\psi(t_j, x_n)$ at time t_j over the truncated set of the lowest $N/2$ Fourier modes propagating to the left and to

the right,

$$\psi(t_j, x_n) \approx \sum_{k=0}^{N/2-1} \beta_k^{(-)} e^{-i \frac{\pi}{R_{\max}} k (x_n + R_{\max})} \quad (\text{A1})$$

$$+ \sum_{k=1}^{N/2} \beta_k^{(+)} e^{i \frac{\pi}{R_{\max}} k (x_n + R_{\max})} \quad (\text{A2})$$

where $\beta_k^{(\pm)}$ are the Fourier amplitudes at time t_j . We apply the FFT to $\psi(t_j, x_n)$ to compute the amplitudes, and use the inverse FFT to compute the second derivative,

$$\partial_{xx} \psi(t_j, x_n) \approx \sum_{k=1}^{N/2-1} - \left(\frac{\pi}{R_{\max}} k \right)^2 \beta_k^{(-)} e^{-i \frac{\pi}{R_{\max}} k (x_n + R_{\max})} \quad (\text{A3})$$

$$+ \sum_{k=1}^{N/2} - \left(\frac{\pi}{R_{\max}} k \right)^2 \beta_k^{(+)} e^{i \frac{\pi}{R_{\max}} k (x_n + R_{\max})}. \quad (\text{A4})$$

Note that the boundary conditions $|\psi(t_j, \pm R_{\max})| \ll 1$ require that $\beta_0^{(-)} \approx 0$ and $\beta_k^{(+)} \approx -\beta_k^{(-)}$. We use these conditions as a quality check in our simulations. Terms on the RHS of the equation that do not involve differentiation are computed using $\psi(t_j, x_n)$.

Our second scheme to simulate NLSEs is similar to that employed in Ref. [46, 83]. It truncates the spatial domain to $x \in [-R_{\max}, R_{\max}]$ as well, and discretizes it to $x_n = R_{\max}(\frac{2n}{N} - 1)$ with $n = 0, 1, \dots, N$. We use, in this case, the finite-difference method to compute spatial derivatives like in Ref. [46, 83], while the 6RK algorithm is used to advance in time. The two schemes have shown an excellent agreement, conserving the norm M (3) and energy H (4), with maximum deviations at the level of the numerical precision $\sim 10^{-13}$ for the first scheme, and $\sim 10^{-13}$ for M , $\sim 10^{-8}$ for H in the second scheme in the HO, while $\sim 10^{-9}$ for M , $\sim 10^{-5}$ for H in the box. The codes have been implemented in C++, running parallel computations on a GPU to speed up the simulation. The number of points that we used varies depending on the initial data and the setup – typically, N ranges from 2^{13} to 2^{17} in the case of the HO potential, and from 2^{11} to 2^{13} in the case of the box potential.

Appendix B: The decay of $S_n(k)$

We show here that amplitudes

$$\mathcal{S}_n(k) \equiv \underbrace{\sum_{m=0}^{\infty} \sum_{i=0}^{\infty} \sum_{j=0}^{\infty} C_{nmij} \bar{\alpha}_m \alpha_i \alpha_j}_{\Delta_{nmij} = \mathcal{W}_k}, \quad (\text{B1})$$

are strongly suppressed at large $|n-k|$ for highly resonant systems,

$$E_n = an + b \quad \text{with} \quad n \in \mathbb{N}, \quad a, b \in \mathbb{R}, \quad (\text{B2})$$

for configurations of α_n that actually occur in the course of the evolution (with an exponential suppression at large n). First, Fig. 7 visually illustrates the fact that the suppression of $\mathcal{S}_n(k)$ at large $|n-k|$ depends very little on the couplings C_{nmij} , irrespective of the decay or growth with the variation of the indices, but, in contrast, it strongly depends on the equidistant relation of eigenvalues (B2). In each plots of Fig. 7 we have numerically calculated the values of $\mathcal{S}_n(k)$, using the same C_{nmij} and α_n but two different choices of eigenvalues, equidistant $E_n = n + 1$ and quadratic $E_n = (n + 1)^2$ ones. This may seem as a minor difference because E_n only affects the computation of expression (B1) through

$$\Delta_{nmij} = E_n + E_m - E_i - E_j, \quad (\text{B3})$$

to restrict the interactions to frequency \mathcal{W}_k . However, it leads to a dramatic difference between the behavior of $\mathcal{S}_n(k)$ at moderate and large values of $|n-k|$ for the equidistant and quadratic energy eigenvalues. As we observe in all the plots of Fig. 7, in the equidistant case these amplitudes rapidly decay with the increase of $|n-k|$ (resembling an exponential decay), while this does not happen in the quadratic case. For those specific plots we have used

$$\alpha_n = (n + 1)^2 e^{-n} \mathcal{A}_n e^{i\mathcal{P}_n}, \quad (\text{B4})$$

$$C_{nmij} = (n + m + i + j + 1)^r, \quad (\text{B5})$$

where \mathcal{A}_n , and \mathcal{P}_n are random variables uniformly distributed on $[0, 1]$ and $[0, 2\pi)$, respectively, power r gave the opportunity to find out if the coefficients decay ($r < 0$), remain constant ($r = 0$), or grow ($r > 0$) with the variation of the indices. Note that expression (B4) captures the qualitative behavior of α_n in our numerical simulation, as explained in Section III. Other choices from this class of conditions lead to the same conclusion. For C_{nmij} we have used the power law in Eq. (B5) because they exhibit, at most, a polynomial growth with the increase of the indices in all physically relevant systems we are aware of. For instance, the D-dimensional GPE with the HO potential has asymptotic values $C_{nnnn} \sim n^{\frac{d}{2}-2}$ for large n [83], and similar asymptotics have been found for relativistic wave equations [93–95]. Other choices of C_{nmij} in this class lead to the same conclusion as well.

We are going to show now that the exponential decay of $\mathcal{S}_n(k)$ for highly resonant systems (B2) may be derived analytically arriving to the expression

$$|\mathcal{S}_n(k)| < e^{-\beta|n-k|} P_{n,k} \quad (\text{B6})$$

where $\beta > 0$, and $P_{n,k}$ is a polynomial in n and k that depends on the detailed form of α_n and C_{nmij} . To derive this bound, we use an estimate for the exponential decay of α_n at large n , which is what actually happens in our simulations, and an arbitrary polynomial $p_n^{(s)}$ in n of degree $s > 0$ to bound different values of α_n . Thus, this estimate has the form of $|\alpha_n| < p_n^{(s)} e^{-\beta n}$ where $\beta > 0$ is not specified and appears in (B6), as we show below.

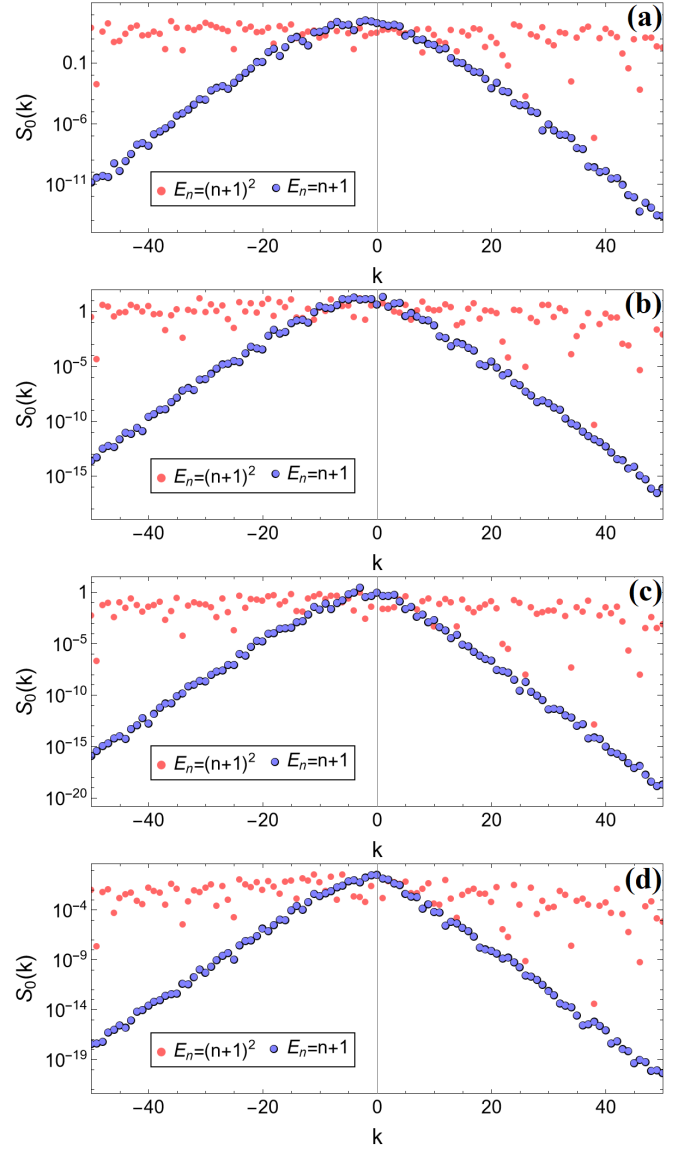


FIG. 7. Comparison between amplitudes $\mathcal{S}_0(k)$ for the linear $E_n = n + 1$ and quadratic $E_n = (n + 1)^2$ spectra of the energy eigenvalues. In each plot, we have used the same α_n and C_{nmij} for both sets of eigenvalues, with the expressions given by (B4)-(B5). The difference between plots is the power of C_{nmij} , $r = 3, 1.5, 0, -1$, from top to bottom.

For the couplings, we are going to use an estimate based on an arbitrary polynomial $q_n^{(r)}$ in n of degree $r > 0$ for each index, $|C_{nmij}| < Q_{nmij}^{(r)} \equiv q_n^{(r)} q_m^{(r)} q_i^{(r)} q_j^{(r)}$. This estimate comes from the observation that the couplings have a polynomial growth at most for large values of the indices, as mentioned above. An estimate admitting each index to have a different power may be used, but it can be covered by the present choice, simply setting r equal to the largest power. Plugging the estimates for α_n and

C_{nmij} into the expressions for $\mathcal{S}_n(k)$ (B1), we obtain

$$\begin{aligned}
|\mathcal{S}_n(k)| &= \left| \sum_{m=0}^{\infty} \sum_{i=0}^{\infty} \sum_{j=0}^{\infty} C_{nmij} \bar{\alpha}_m \alpha_i \alpha_j \right| \quad (\text{B7}) \\
&< \underbrace{\sum_{m=0}^{\infty} \sum_{i=0}^{\infty} \sum_{j=0}^{\infty}}_{n+m-i-j=k} |C_{nmij}| |\bar{\alpha}_m| |\alpha_i| |\alpha_j| \\
&< \underbrace{\sum_{m=0}^{\infty} \sum_{i=0}^{\infty} \sum_{j=0}^{\infty}}_{n+m-i-j=k} Q_{nmij}^{(r)} p_m^{(s)} p_i^{(s)} p_j^{(s)} e^{-\beta(m+i+j)}.
\end{aligned}$$

The constraint on the indices, $n + m - i - j = k$, may be used to remove the summation in j . Two cases must be distinguished, *viz.*, $k < n$ and $k \geq n$, to guarantee that $j \geq 0$.

Case $k < n$: Substituting $j = n + m - k - i$ one gets

$$\begin{aligned}
|\mathcal{S}_n(k)| &< e^{\beta(k-n)} \sum_{m=0}^{\infty} e^{-2\beta m} p_m^{(s)} \quad (\text{B8}) \\
&\times \sum_{i=0}^{n-k+m} Q_{nmi(n-k+m-i)}^{(r)} p_i^{(s)} p_{(n-k+m-i)}^{(s)}.
\end{aligned}$$

We know that the sum $\sum_{i=1}^M i^a$ with $a \geq 0$ is a polynomial of degree $a + 1$ in M [96]. Then, the summation in index i is a polynomial n, m , and k , denoted by $F_{n,m,k}$. We use now that $\sum_{m=0}^{\infty} e^{-2\beta m} (m+1)^b$ with $b \in \mathbb{R}$ and $\beta > 0$ is a finite number to get

$$|\mathcal{S}_n(k)| < e^{\beta(k-n)} \sum_{m=0}^{\infty} e^{-2\beta m} p_m^{(s)} F_{n,m,k} < P_{n,k} e^{\beta(k-n)} \quad (\text{B9})$$

where $P_{n,k}$ is a polynomial in n and k respectively.

Case $k \geq n$: In this case one has to be careful with the ranges of m and i to guarantee that $j \geq 0$. Taking this into account, the expression for $\mathcal{S}_n(k)$ is

$$\begin{aligned}
|\mathcal{S}_n(k)| &< e^{\beta(k-n)} \sum_{m=k-n}^{\infty} e^{-2\beta m} p_m^{(s)} \quad (\text{B10}) \\
&\times \sum_{i=0}^{n-k+m} Q_{nmi(n-k+m-i)}^{(r)} p_i^{(s)} p_{(n-k+m-i)}^{(s)} \\
&= e^{\beta N} \sum_{M=0}^{\infty} e^{-2\beta M} p_{M+N}^{(s)} \sum_{i=0}^M Q_{n(M+N)i(M-i)}^{(r)} p_i^{(s)} p_{(M-i)}^{(s)}.
\end{aligned}$$

where we have made the following changes, $N = n - k$ and $M = m + N$, in order to remove the dependence of the lowest value of m on $k - n$. Note that these changes flipped the sign in the first exponential. The resulting expression is similar to the one for the case of $k < n$, and we proceed using the same properties to conclude that

$$|\mathcal{S}_n(k)| < e^{\beta(n-k)} P_{n,k}, \quad (\text{B11})$$

where in this case $P_{n,k}$ is a polynomial in n and k . The combination of Eqs. (B9) for $k < n$ and (B11) for $k \geq n$ results in Eq. (B6).

One may try to derive an estimate similar to Eq. (B1) for case of the box potential, but the quadratic eigenvalues (9) make this process much more difficult than in the case of the equidistant eigenvalues. The difficulties appear in the constraint imposed on the indices (B3),

$$k = (n+1)^2 + (m+1)^2 - (i+1)^2 - (j+1)^2. \quad (\text{B12})$$

However, for very high frequencies ($|k| \gg n^2$), using the above-mentioned estimates $|\alpha_n| < p_n^{(s)} e^{-\beta n}$, and $|C_{nmij}| < q_n^{(r)} q_k^{(r)} q_i^{(r)} q_j^{(r)}$ one may see that

$$|\mathcal{S}_n(k)| \underset{|k| \gg n^2}{<} D_{n,k} e^{-\beta \sqrt{|k|}}, \quad (\text{B13})$$

where $D_{n,k}$ is a polynomial in n and k , and β is again the exponent of $|\alpha_n|$. Note that in this case the suppression of high frequencies ($k \gg n^2$) is much weaker than for the equidistant energy spectrum. This estimate comes from assessing the dominant contribution of k in different terms of $|\mathcal{S}_n(k)|$ according to Eq. (B1),

$$|C_{nmij}| |\bar{\alpha}_m| |\alpha_i| |\alpha_j| < Q_{nmij}^{(r)} p_m^{(s)} p_i^{(s)} p_j^{(s)} e^{-\beta(m+i+j)}. \quad (\text{B14})$$

The key part of this expression is the $\exp[-\beta(m+i+j)]$. To confirm its dominance for very high frequencies $k \gg n^2$, we use the relation (B12) between the indices, to obtain

$$m = \sqrt{k - (n+1)^2 + (i+1)^2 + (j+1)^2} - 1. \quad (\text{B15})$$

Plugging this expression in the exponential and assuming that $k > 0$ ($k < 0$ is similar), one arrives to the following asymptotic expressions:

Case $k \gg i^2, j^2, n^2$:

$$-\beta(m+i+j) \sim -\beta \sqrt{k} - \beta(i+j-1) + \mathcal{O}\left(\frac{1}{\sqrt{k}}\right). \quad (\text{B16})$$

Then, the sums in $\mathcal{S}_n(k)$ that cover the range of $k \gg i^2, j^2, n^2$ may be bounded as

$$\begin{aligned}
&\sum_{i=0}^{\infty} \sum_{j=0}^{\infty} Q_{nmij}^{(r)} p_m^{(s)} p_i^{(s)} p_j^{(s)} e^{-\beta(m+i+j)} \quad (\text{B17}) \\
&\leq e^{-\beta \sqrt{k}} \sum_{i=0}^{\infty} \sum_{j=0}^{\infty} Q_{nmij}^{(r)} p_m^{(s)} p_i^{(s)} p_j^{(s)} c e^{-\beta(i+j)} \\
&\leq D_{n,k} e^{-\beta \sqrt{k}},
\end{aligned}$$

where $D_{n,k}$ is a polynomial in n, k , and we have used the following properties to reach the last expression. First, we used constant c large enough to bound the independent term and terms $\mathcal{O}\left(\frac{1}{\sqrt{k}}\right)$ in the exponent. We also used the fact that $\sum_{i=0}^{\infty} e^{-\beta i} (i+1)^b$ with $b \in \mathbb{R}$ and $\beta > 0$ takes a finite value to bound the sums in the intermediate expression independently of the upper limit. Finally, we

used a polynomial $D_{n,k}$ of high enough degree to bound the terms involving n and k .

Case $i^2 \sim j^2 \sim k \gg n^2$:

$$\begin{aligned} -\beta(m+i+j) &\sim -\beta\sqrt{k} - \beta(i+j) \\ +\beta\left(1 - \frac{i+j}{\sqrt{i^2+j^2+k}}\right) &+ \beta\mathcal{O}\left(\frac{1}{\sqrt{k}}\right). \end{aligned} \quad (\text{B18})$$

We proceed in the same way as in the case of Eq. (B17). One just needs to note that, after the exponentiation, the third term in the exponent may be bounded by a constant because

$$\beta\left(1 - \frac{i+j}{\sqrt{i^2+j^2+k}}\right) \leq \beta. \quad (\text{B19})$$

Then, after following the same steps, we arrive at the bound $D_{n,k}e^{-\beta\sqrt{k}}$.

Case $j^2 \sim i^2 \gg k \gg n^2$:

$$\begin{aligned} -\beta(m+i+j) &\sim -\beta(i+j) - \beta\left(\sqrt{i^2+j^2}\right) \\ +\beta\left(1 - \frac{i+j}{\sqrt{i^2+j^2}}\right) &+ \mathcal{O}\left(\frac{1}{i}\right) + \mathcal{O}\left(\frac{1}{j}\right). \end{aligned} \quad (\text{B20})$$

For the second term we use the bound

$$-\beta\left(\sqrt{i^2+j^2}\right) \ll -\beta\left(\sqrt{2k}\right) < -\beta\left(\sqrt{k}\right), \quad (\text{B21})$$

while the third term is bounded by a constant

$$\beta\left(1 - \frac{i+j}{\sqrt{i^2+j^2}}\right) \leq \beta. \quad (\text{B22})$$

Again, proceeding like in the case of Eq. (B17), we get the bound $D_{n,k}e^{-\beta\sqrt{k}}$.

We have shown here how to establish a bound on the sums in $\mathcal{S}_n(k)$ under three of the most important relations between $\{i, j, k\}$. For other relations, as $i^2 \gg k \gg n^2$, j^2 , one has to proceed in the same way as we have illustrated here to obtain the bound $D_{n,k}e^{-\beta\sqrt{k}}$. For the case of $k < 0$ the process is the same, one just needs to take into account that some relations between the indices and k do not lead to $m \geq 0$ and are therefore excluded. For instance, the equivalent of the first regime that we have addressed, $|k| \gg i^2, j^2, n^2$, is no longer present because m would be an imaginary number (B15). After bounding all the regimes one arrives at estimate (B13) for $|\mathcal{S}_n(k)|$ in the case of the box potential.

Appendix C: Eigenstates

We collect here results for the Schrödinger equations introduced in the main text. The results for the 1D Schrödinger equation with the HO and box potentials are provided above in Eqs. (8)-(9).

Schrödinger equation (29) with the HO potential in D dimensions:

$$E_n = 2n + \frac{D}{2}, \quad (\text{C1})$$

$$f_n(r) = \sqrt{\frac{n!\Gamma(D/2)}{\pi^{d/2}\Gamma(n+D/2)}} L_n^{(D/2)}(r^2) e^{-r^2/2}, \quad (\text{C2})$$

where $L_n^{(\alpha)}$ are the generalized Laguerre polynomials. **1D Schrödinger equation with potential $V^{(1)}(x)$ (30):**

$$E_n = 2n + \frac{\delta}{2}, \quad (\text{C3})$$

$$f_n(x) = \sqrt{\frac{n!\Gamma(\delta/2)}{\pi^{\delta/2}\Gamma(n+\delta/2)}} L_n^{(\delta/2)}(r^2) e^{-x^2/2}, \quad (\text{C4})$$

where $\delta = 2 + \sqrt{1+4s}$ and $L_n^{(\alpha)}(x)$ are the generalized Laguerre polynomials.

We also show here how to derive the 1D-GPE with potential $V^{(1)}$, (30), from the dimensional reduction of the following D-dimensional NLSE with the HO potential:

$$i\partial_t\psi = \frac{1}{2}\left(-\partial_{rr} - \frac{D-1}{r}\partial_r + r^2\right)\psi + gr^{D-1}|\psi|^2\psi, \quad (\text{C5})$$

with $r \in [0, \infty)$, and the nonlinear term has the factor r^{D-1} . First, one has to plug the change $\psi(t, x) = r^{\frac{1-D}{2}}\tilde{\psi}(t, r)$ into the equation to get rid of the first-differentiation terms. Then, one extracts the factor $r^{\frac{1-D}{2}}$ from the RHS and LHS to get

$$i\partial_t\tilde{\psi} = -\frac{1}{2}\partial_{rr}\tilde{\psi} + \left(\frac{r^2}{2} + \frac{D^2-4D+3}{8r^2}\right)\tilde{\psi} + g|\tilde{\psi}|^2\tilde{\psi}, \quad (\text{C6})$$

which is the 1D-GPE with the anharmonic potential $V^{(1)}$ (30) on the half-line.

1D-Schrödinger equation with potential $V^{(2)}(x)$ (31):

$$E_n = 2n + \frac{23}{6}, \quad (\text{C7})$$

$$f_n(x) = \frac{2^{n+1/2}n!}{\pi^{1/4}\sqrt{(2n+5)(2n+1)(2n)!}} e^{-x^2/2} \quad (\text{C8})$$

$$\times \left(\frac{3(1+2x^2)}{(3+2x^2)} L_n^{(1/2)}(x^2) - 2(n+1)L_{n+1}^{(-1/2)}(x^2)\right), \quad (\text{C9})$$

where $L_n^{(\alpha)}(x)$ are the generalized Laguerre polynomials. **1D-Schrödinger equation with potential $V^{(3)}(x)$ (32):**

$$E_0 = -\frac{5}{6}, \quad E_{n \geq 1} = n + \frac{7}{6}, \quad (\text{C10})$$

$$f_0(x) = \frac{\sqrt{2}}{\pi^{1/4}} \frac{e^{-x^2/2}}{1+2x^2}, \quad (\text{C11})$$

$$f_{n \geq 1}(x) = \frac{1}{\pi^{1/4} \sqrt{2^n(n+2)(n-1)!}} e^{-x^2/2} \quad (\text{C12})$$

$$\times \left(\frac{4x}{(1+2x^2)} H_{n-1}(x) + H_n(x) \right). \quad (\text{C13})$$

where $H_n(x)$ are the Hermite polynomials.

1D-Schrödinger equation with potential $V^{(4)}(x)$ (33):

$$E_0 = -\frac{3}{2}, \quad E_{n \geq 1} = n + \frac{5}{2}, \quad (\text{C14})$$

$$f_0(x) = \frac{2\sqrt{6}}{\pi^{1/4}} \frac{e^{-x^2/2}}{3+12x^2+4x^4}, \quad (\text{C15})$$

$$f_{n \geq 1}(x) = \frac{1}{\pi^{1/4} \sqrt{2^n(n+4)(n-1)!}} e^{-x^2/2} \quad (\text{C16})$$

$$\times \left(\frac{8x(3+2x^2)}{(3+12x^2+4x^4)} H_{n-1}(x) + H_n(x) \right), \quad (\text{C17})$$

where $H_n(x)$ are the Hermite polynomials.

Two-component 1D Schrödinger equation (37): Using transformation $\psi_+ = u + v$ and $\psi_- = u - v$, the equation produces two “towers” of eigenvalues,

$$E_n^{(\pm)} = n + \frac{1}{2} \pm c, \quad (\text{C18})$$

and the same eigenfunctions as above:

$$f_n^{(\pm)}(x) = \frac{1}{\pi^{1/4} \sqrt{2^n n!}} H_n(x) e^{-x^2/2}. \quad (\text{C19})$$

A wave equation in the anti-de Sitter space (38):

$$E_n = 2n + 3, \quad (\text{C20})$$

$$f_n(x) = \frac{2\sqrt{n!(n+2)!}}{\Gamma(n+\frac{3}{2})} \cos^3(x), P^{(\frac{1}{2}, \frac{3}{2})}(\cos 2x), \quad (\text{C21})$$

where $P^{(\frac{1}{2}, \frac{3}{2})}$ are Jacobi polynomials.

-
- [1] S. B. Kuksin, *Nearly integrable infinite-dimensional Hamiltonian systems*, Lecture Notes in Mathematics, vol. **1556**, Springer, Berlin (1993).
- [2] A. J. Lichtenberg, and M. A. Lieberman, *Regular and stochastic motion*, vol. **38**, Springer Science & Business Media, 1983.
- [3] B. Paredes, A. Widera, V. Murg, O. Mandel, S. Fölling, I. Cirac, G. V. Shlyapnikov, T. W. Hansch, and I. Bloch, *Tonks-Girardeau gas of ultracold atoms in an optical lattice*, Nature **429**, 277-281 (2004).
- [4] T. Kinoshita, T. Wenger, and D. S. Weiss, *A quantum Newton’s cradle*, Nature (London) **440**, 900 (2006).
- [5] E. H. Lieb and W. Liniger, *Exact Analysis of an Interacting Bose Gas. I. The General Solution and the Ground State*, Phys. Rev. **130**, 1605 (1963).
- [6] T. Langen, R. Geiger, and J. Schmiedmayer, *Ultracold atoms out of equilibrium*, Annu. Rev. Condens. Matter Phys., **6**, 201-217 (2015).
- [7] B. Bertini, M. Collura, J. De Nardis, and M. Fagotti, *Transport in out-of-equilibrium XXZ chains: Exact profiles of charges and currents*, Phys. Rev. Lett., **117**, 207201 (2016).
- [8] O. A. Castro-Alvaredo, B. Doyon, and T. Yoshimura, *Emergent hydrodynamics in integrable quantum systems out of equilibrium*, Phys. Rev. X, **6**, 041065 (2016).
- [9] A. Bastianello, A. De Luca, and R. Vasseur, *Hydrodynamics of weak integrability breaking*, Journal of Statistical Mechanics: Theory and Experiment, **2021**(11), 114003 (2021).
- [10] I. Bouchoule, and J. Dubail, *Generalized hydrodynamics in the one-dimensional Bose gas: theory and experiments*, Journal of Statistical Mechanics: Theory and Experiment, **2022**, 014003 (2022).
- [11] A. Bastianello, A. De Luca, B. Doyon, and J. De Nardis, *Thermalization of a trapped one-dimensional Bose gas via diffusion*, Phys. Rev. Lett., **125**, 240604 (2020).
- [12] F. Møller, C. Li, I. Mazets, H.-P. Stimming, T. Zhou, Z. Zhu, X. Chen, and J. Schmiedmayer, *Extension of the Generalized Hydrodynamics to the Dimensional Crossover Regime*, Phys. Rev. Lett. **126**, 090602 (2021).
- [13] N. Malvania, Y. Zhang, Y. Le, J. Dubail, M. Rigol, and D. S. Weiss, *Generalized hydrodynamics in strongly interacting 1D Bose gases*, Science, **373**, 1129-1133 (2021).
- [14] M. Gring, M. Kuhnert, T. Langen, T. Kitagawa, B. Rauer, M. Schreitl, I. Mazets, D. Adu Smith, E. Demler, and J. Schmiedmayer, *Relaxation and Prethermalization in an Isolated Quantum System*, Science **337**, 1318 (2012).
- [15] D. Adu Smith, M. Gring, T. Langen, M. Kuhnert, B. Rauer, R. Geiger, T. Kitagawa, I. Mazets, E. Demler, and J. Schmiedmayer, *Prethermalization Revealed by the Relaxation Dynamics of Full Distribution Functions*, New J. Phys. **15**, 075011 (2013).
- [16] T. Langen, S. Erne, R. Geiger, B. Rauer, T. Schweigler, M. Kuhnert, W. Rohringer, I. E. Mazets, T. Gasenzer, and J. Schmiedmayer, *Experimental Observation of a Generalized Gibbs Ensemble*, Science **348**, 207 (2015).
- [17] Y. Tang, W. Kao, K. Y. Li, S. Seo, K. Mallayya, M. Rigol,

- M., S. Gopalakrishnan, and B. L. Lev, *Thermalization near integrability in a dipolar quantum Newton's cradle*, Phys. Rev. X, **8**, 021030 (2018).
- [18] M. Rigol, V. Dunjko, V. Yurovsky, and M. Olshanii, *Relaxation in a completely integrable many-body quantum system: an ab initio study of the dynamics of the highly excited states of 1D lattice hard-core bosons*, Phys. Rev. Lett. **98**, 050405 (2007).
- [19] L. Vidmar, and M. Rigol, *Generalized Gibbs ensemble in integrable lattice models*, Journal of Statistical Mechanics: Theory and Experiment, **2016**(6), 064007 (2016).
- [20] B. Doyon, *Thermalization and Pseudolocality in Extended Quantum Systems*, Commun. Math. Phys. **351**, 155-200 (2017).
- [21] X. Cao, V. B. Bulchandani, and J. E. Moore, *Incomplete thermalization from trap-induced integrability breaking: Lessons from classical hard rods*, Phys. Rev. Lett., **120**, 164101 (2018).
- [22] A. Hutsalyuk, and B. Pozsgay, *Integrability breaking in the one-dimensional Bose gas: Atomic losses and energy loss*, Phys. Rev. E, **103**, 042121 (2021).
- [23] K. F. Thomas, M. J. Davis, and K. V. Kheruntsyan, *Thermalization of a quantum Newton's cradle in a one-dimensional quasicondensate*, Phys. Rev. A **103**, 023315 (2021).
- [24] A. V. Turbinger, *One-dimensional quasi-exactly solvable Schrödinger equations*, Phys. Rep. **642**, 1-71 (2016).
- [25] P. Villain, and M. Lewenstein, *Fermi-Pasta-Ulam problem revisited with a Bose-Einstein condensate*, Physical Review A, **62**, 043601 (2000).
- [26] E. P. Gross, *Structure of a quantized vortex in boson systems*, Nuovo Cim. **20**, 454 (1961).
- [27] L. P. Pitaevskii, *Vortex Lines in an Imperfect Bose Gas*, Soviet J. Exp. Theor. Phys. **13**, 451 (1961).
- [28] L. Pitaevskii, and S. Stringari, *Bose Einstein Condensation*, Oxford University Press: Oxford, UK, 2003.
- [29] C. J. Pethick, and H. Smith, *Bose-Einstein Condensation in Dilute Gases*, Cambridge University Press: Cambridge, UK, 2001.
- [30] C. F. Barenghi, and N. G. Parker, *A Primer on Quantum Fluids*, Springer: Berlin, Germany, 2017.
- [31] V. E. Zakharov, and A. B. Shabat, *Exact Theory of Two-dimensional Self-focusing and One-dimensional Self-modulation of Waves in Nonlinear Media*, Zh. Eksp. Teor. Fiz. **61**, 118-134 (1971).
- [32] V. E. Zakharov, and S. V. Manakov, *On the complete integrability of a nonlinear Schrödinger equation*, Theoretical and Mathematical Physics, **19**, 551-559 (1974).
- [33] Yu. S. Kivshar and B. A. Malomed, *Dynamics of solitons in nearly integrable systems*, Rev. Mod. Phys. **61**, 763 (1989).
- [34] I. Březinová, L. A. Collins, K. Ludwig, B. I. Schneider, and J. Burgdörfer, *Wave chaos in the nonequilibrium dynamics of the Gross-Pitaevskii equation*, Phys. Rev. A, **83**, 043611 (2011).
- [35] I. Březinová, A. U. Lode, A. I. Streltsov, O. E. Alon, L. S. Cederbaum, and J. Burgdörfer, *Wave chaos as signature for depletion of a Bose-Einstein condensate*, Phys. Rev. A **86**, 013630 (2012).
- [36] S. Donsa, H. Hofstätter, O. Koch, J. Burgdörfer, and I. Březinová, *Long-time expansion of a Bose-Einstein condensate: Observability of Anderson localization*, Phys. Rev. A, **96**, 043630 (2017).
- [37] L. Ermann, E. Vergini, and D. L. Shepelyansky, *Dynamics and thermalization of a Bose-Einstein condensate in a Sinai-oscillator trap*, Phys. Rev. A, **94**, 013618 (2016).
- [38] J. Ruostekoski, B. Kneer, W. P. Schleich, and G. Remppe, *Interference of a Bose-Einstein condensate in a hard-wall trap: From the nonlinear Talbot effect to the formation of vorticity*, Phys. Rev. A, **63**, 043613 (2001).
- [39] S. P. Cockburn, A. Negretti, N. P. Proukakis, C. Henkel, *Comparison between microscopic methods for finite-temperature Bose gases*, Phys. Rev. A, **83**, 043619 (2011).
- [40] S. P. Cockburn, D. Gallucci, and N. P. Proukakis, *Quantitative study of quasi-one-dimensional Bose gas experiments via the stochastic Gross-Pitaevskii equation*, Phys. Rev. A, **84**, 023613 (2011).
- [41] Y. Kagan, E. L. Surkov, and G. V. Shlyapnikov, *Evolution of a Bose-condensed gas under variations of the confining potential*, Physical Review A, **54**, R1753 (1996).
- [42] P. A. Ruprecht, M. J. Holland, K. Burnett, and M. Edwards, *Time-dependent solution of the nonlinear Schrödinger equation for Bose-condensed trapped neutral atoms*, Phys. Rev. A **51**, 4704 (1995).
- [43] N. G. Parker, N. P. Proukakis, C. G. Barenghi, C. S. Adams, *Dynamical instability of a dark soliton in a quasi-one-dimensional Bose-Einstein condensate perturbed by an optical lattice*, Journal of Physics B: Atomic, Molecular and Optical Physics, **37**, S175 (2004).
- [44] N. G. Parker, N. P. Proukakis, and C. S. Adams, *Dark soliton decay due to trap anharmonicity in atomic Bose-Einstein condensates*, Phys. Rev. A, **81**, 033606 (2010).
- [45] N. G. Parker, N. P. Proukakis, M. Leadbeater, and C. S. Adams, *Soliton-sound interactions in quasi-one-dimensional Bose-Einstein condensates*, Phys. Rev. Lett., **90**, 220401 (2003).
- [46] T. Bland, N. G. Parker, N. P. Proukakis, and B. A. Malomed, *Probing quasi-integrability of the Gross-Pitaevskii equation in a harmonic-oscillator potential*, J. Phys. B: At. Mol. Opt. Phys. **51**, 205303 (2018).
- [47] A. D. Martin, C. S. Adams, and S. A. Gardiner, *Bright solitary-matter-wave collisions in a harmonic trap: Regimes of solitonlike behavior*, Phys. Rev. A, **77**, 013620 (2008).
- [48] A. Weller, J. P. Ronzheimer, C. Gross, J. Esteve, M. K. Oberthaler, D. J. Frantzeskakis, G. Theocharis, and P. G. Kevrekidis, *Experimental observation of oscillating and interacting matter wave dark solitons*, Phys. Rev. Lett., **101**, 130401 (2008).
- [49] C. Becker, S. Stellmer, P. Soltan-Panahi, S. Dörscher, M. Baumert, E. M. Richter, J. Kronjäger, K. Bongs, and K. Sengstock, *Oscillations and interactions of dark and dark-bright solitons in Bose-Einstein condensates*, Nature Physics, **4**, 496-501 (2008).
- [50] T. Busch, and J. R. Anglin, *Motion of dark solitons in trapped Bose-Einstein condensates*, Phys. Rev. Lett., **84**, 2298 (2000).
- [51] G. Huang, J. Szeftel, and S. Zhu, *Dynamics of dark solitons in quasi-one-dimensional Bose-Einstein condensates*, Phys. Rev. A, **65**, 053605 (2002).
- [52] D. J. Frantzeskakis, *Dark solitons in atomic Bose-Einstein condensates: from theory to experiments*, Journal of Physics A: Mathematical and Theoretical, **43**, 213001 (2010).
- [53] Y. Castin, and R. Dum, *Bose-Einstein condensates in time dependent traps*, Phys. Rev. Lett., **77**, 5315 (1996).
- [54] Y. Kagan, E. L. Surkov, and G. V. Shlyapnikov, *Evolution of a Bose gas in anisotropic time-dependent traps*,

- Physical Review A, **55**, R18 (1997).
- [55] A. Sinatra, P. O. Fedichev, Y. Castin, J. Dalibard, and G. V. Shlyapnikov, *Dynamics of two interacting Bose-Einstein condensates*, Phys. Rev. Lett., **82**, 251 (1999).
- [56] F. Dalfovo, S. Giorgini, L. P. Pitaevskii, and S. Stringari, *Theory of Bose-Einstein condensation in trapped gases*, Reviews of modern physics, **71**, 463 (1999).
- [57] K. Góral, M. Gajda, and K. Rzȃzewski, *Thermodynamics of an interacting trapped Bose-Einstein gas in the classical field approximation*, Phys. Rev. A, **66**, 051602 (2002).
- [58] B. Damski, and W. H. Zurek, *Soliton creation during a Bose-Einstein condensation*, Phys. Rev. Lett., **104**, 160404 (2010).
- [59] P. Grisins, and I. E. Mazets, *Thermalization in a one-dimensional integrable system*, Phys. Rev. A, **84**, 053635 (2011).
- [60] S. Burger, K. Bongs, S. Dettmer, W. Ertmer, K. Sengstock, A. Sanpera, G. V. Shlyapnikov, and M. Lewenstein, *Dark solitons in Bose-Einstein condensates*, Phys. Rev. Lett., **83**, 5198 (1999).
- [61] V. Shukla, S. Nazarenko, *Nonequilibrium Bose-Einstein condensation*, Phys. Rev. A, **105**, 033305 (2022).
- [62] A. Biasi, P. Bizoń, B. Craps and O. Evnin, *Exact lowest-Landau-level solutions for vortex precession in Bose-Einstein condensates*, Phys. Rev. A **96**, 053615 (2017).
- [63] P. Gérard, P. Germain and L. Thomann, *On the cubic lowest Landau level equation*, Arch. Rat. Mech. Anal. **231**, 1073 (2019).
- [64] A. Biasi, P. Bizoń, B. Craps and O. Evnin, *Two infinite families of resonant solutions for the Gross-Pitaevskii equation*, Phys. Rev. E **98**, 032222 (2018).
- [65] A. Biasi, O. Evnin, and B. A. Malomed, *Fermi-Pasta-Ulam phenomena and persistent breathers in the harmonic trap*, Phys. Rev. E, **104**, 034210 (2021).
- [66] A. Biasi, P. Bizoń and O. Evnin, *Solvable cubic resonant systems*, Comm. Math. Phys. **369**, 433 (2019).
- [67] O. Evnin, *Breathing modes, quartic nonlinearities and effective resonant systems*, SIGMA **16**, 034 (2020).
- [68] L. P. Pitaevskii, *Dynamics of collapse of a confined Bose gas*, Phys. Lett. A **221**, 14-18 (1996).
- [69] L. P. Pitaevskii, A. Rosch, *Breathing modes and hidden symmetry of trapped atoms in two dimensions*, Phys. Rev. A **55**, R853-856 (1997).
- [70] A. Biasi, P. Bizoń and O. Evnin, *Complex plane representations and stationary states in cubic and quintic resonant systems*, J. Phys. A **52**, 435201 (2019).
- [71] S. Nazarenko, *Wave turbulence*, Springer Science & Business Media, 2011.
- [72] P. Walczak, S. Randoux, and P. Suret, *Optical rogue waves in integrable turbulence*, Phys. Rev. Lett., **114**, 143903 (2015).
- [73] S. Randoux, P. Walczak, M. Onorato, and P. Suret, *Nonlinear random optical waves: Integrable turbulence, rogue waves and intermittency*, Physica D: Nonlinear Phenomena, **333**, 323-335 (2016).
- [74] D. S. Agafontsev, S. Randoux, and P. Suret, *Extreme rogue wave generation from narrowband partially coherent waves*, Physical Review E, **103**, 032209 (2021).
- [75] V. E. Zakharov, *Turbulence in integrable systems*, Studies in Applied Mathematics, **122**, 219-234, (2009).
- [76] D. S. Agafontsev, and V. E. Zakharov, *Integrable turbulence and formation of rogue waves*, Nonlinearity, **28**, 2791 (2015).
- [77] A. A. Gelash, and D. S. Agafontsev, *Strongly interacting soliton gas and formation of rogue waves*, Physical Review E, **98**, 042210, (2018).
- [78] M. A. Garrido, R. Grande, K. M. Kurianski, and G. Staffilani, *Large deviations principle for the cubic NLS equation*, arXiv:2110.15748 [math.AP].
- [79] A. El Gennady, *Soliton gas in integrable dispersive hydrodynamics*, Journal of Statistical Mechanics: Theory and Experiment, **2021**, 114001 (2021).
- [80] J. A. Murdock, *Perturbations: Theory and Methods*, Wiley, New York, 1991.
- [81] P. Germain, Z. Hani, and L. Thomann, *On the continuous resonant equation for NLS. I. Deterministic analysis*, J. Math. Pure Appl. **105**, 131 (2016).
- [82] F. Kh. Abdullaev and M. Salerno, *Gap-Townes solitons and localized excitations in low-dimensional Bose-Einstein condensate in optical lattices*, Phys. Rev. A **72**, 033617 (2005).
- [83] A. F. Biasi, J. Mas and A. Paredes, *Delayed collapses of BECs in relation to AdS gravity*, Phys. Rev. E **95**, 032216 (2017).
- [84] S. Yu Dubov, V. M. Eleonskii, and N. E. Kulagin, *Equidistant spectra of anharmonic oscillators*, Chaos: An Interdisciplinary Journal of Nonlinear Science **4.1**, 47-53 (1994).
- [85] J. Williams, R. Walser, J. Cooper, E. Cornell, and M. Holland, *Nonlinear Josephson-type oscillations of a driven, two-component Bose-Einstein condensate*, Phys. Rev. A, **59**, R31 (1999).
- [86] N. Hacker, and B. A. Malomed, *Nonlinear dynamics of wave packets in tunnel-coupled harmonic-oscillator traps*, Symmetry, **13**, 372 (2021).
- [87] N. Hacker, and .A. Malomed, *Trapping wave fields in an expulsive potential by means of linear coupling*, Physical Review E, **105**, 034213 (2022).
- [88] M. C. Dos Santos, and W. B .Cardoso, *Anderson localization induced by interaction in linearly coupled binary Bose-Einstein condensates*, Physical Review E, **103**, 052210 (2021).
- [89] P. Bizoń, O. Evnin and F. Ficek, *A nonrelativistic limit for AdS perturbations*, JHEP **12**, 113 (2018).
- [90] O. Evnin, *Resonant Hamiltonian systems and weakly nonlinear dynamics in AdS spacetimes*, Classical and Quantum Gravity, **38**, 203001 (2021).
- [91] V. Zakharov, F. Dias, and A. Pushkarev, *One-dimensional wave turbulence*, Physics Reports, **398**, 1-65, (2004).
- [92] J. Amette Estrada, M. E. Brachet, and P. D. Mininni, *Turbulence in rotating Bose-Einstein condensates*, Phys. Rev. A **105**, 063321 (2022).
- [93] B. Craps, O. Evnin, and J. Vanhoof, *Ultraviolet asymptotics and singular dynamics of AdS perturbations*, JHEP **10**, 079 (2015).
- [94] B. Craps, O. Evnin, P. Jai-akson and J. Vanhoof, *Ultraviolet asymptotics for quasiperiodic AdS₄ perturbations*, JHEP **10**, 080 (2015).
- [95] O. Evnin and P. Jai-akson, *Detailed ultraviolet asymptotics for AdS scalar field perturbations*, JHEP **04**, 054 (2016).
- [96] I. S. Gradshteyn, and I. M. Ryzhik, *Table of Integrals, Series, and Products*, 7th ed. Elsevier, 2007.